TECHNISCHE UNIVERSITÄT WIEN
Vienna University of Technology

UNIKLINIKUM SALZBURG
LANDESKRANKENHAUS

Diplomarbeit, SS 2023/24

Evaluierung von Validierungsparameter zur Erzeugung von hochmodelierten Bestrahlungslänen

zur Erlangung des akademischen Grades

Diplom-Ingenieur

Manuel Wolfgang Schürrer, BSc
Matr.Nr.:11703501

Betreut von:

Ao.Univ.Prof. Dipl.-Ing. Dr. techn. Christina Streli	Ass.Prof. Dipl.-Ing. Dr. techn. Karin Poljanc	Dipl.-Ing. Dr. Christoph Gaisberger

TECHNISCHE UNIVERSITÄT WIEN
Vienna University of Technology

UNIKLINIKUM SALZBURG
LANDESKRANKENHAUS

Diploma thesis, SS 2023/24

Evaluation of validation parameters for generating highly modeled irradiation plans

in fulfillment of the academic degree

Diplom-Ingenieur

Manuel Wolfgang Schürrer, BSc
Matr.Nr.:11703501

Supervised by:

Ao.Univ.Prof. Dipl.-Ing. Dr. techn. Christina Streli	Ass.Prof. Dipl.-Ing. Dr. techn. Karin Poljanc	Dipl.-Ing. Dr. Christoph Gaisberger

Abstract

Radiation therapy is always an evolving field of medical physics and plays an enormous role in the local control of malignant tumors. The most common technique for a radiation therapy in the last few years is the photon-based intensity modeled radiation therapy (IMRT) which can be delivered using a clinical linear accelerator (LINAC). This diploma thesis deals with the evaluation of some planning parameters of these LINACs, in particular the gantry spacing, dynamic and dosimetric properties of the Multi-Leaf Collimator (MLC). To evaluate and validate IMRT plans, the Modulation Complexity Score (MCS) factor and the gamma index based on phantom measurements are used. Therefore, a better understanding of these parameters is crucial to ensure the accuracy and complexity of such plans. Through a comparative analysis of different combinations, this work aims to evaluate the influence of plan complexity on the real applicability of irradiation by the LINAC and to differentiate by varying these parameters. Therefore, 15 realistic treatment plans - five each for prostate, breast (mamma) and head and neck (ENT) tumors - are analyzed and each plan is repeatedly optimized. In addition, the MCS is recalculated each time to assess the impact on plan complexity. In addition, measurements are taken on a phantom (Delta4+, Scanidos, SWE) in order to compare or validate the calculated parameters of the plans. The results of the work contribute to this field by providing a clearer understanding of how different optimization parameters affect the complexity of realistic radiotherapy plans and their dosimetric applicability.

Kurzfassung

Die Strahlentherapie ist ein sich ständig weiterentwickelndes Gebiet der Medizinphysik und spielt eine entscheidende Rolle in der lokalen Kontrolle von malignen Tumoren. Die derzeit gebräuchlichste Technik für eine Strahlentherapie ist die photonenbasierte intensitätsmodolierte Bestrahlungsmethode (IMRT). Sie wird mit Hilfe eines klinischen Linearbeschleuniger (LINAC) durchgeführt. Diese Diplomarbeit beschäftigt sich mit der Analyse einiger relevanter technischer Parameter von LINACs, im speziellen dem Gantry-Spacing und den dynamischen und dosimetrischen Eigenschaften des Multi-Leaf-Kollimators (MLC). Zur Bewertung und Validierung von IMRT Plänen werden der Modulation Complexity Score (MCS)-Faktor und der Gamma-Index basierend auf Phantommessungen verwendet. Durch eine vergleichende Analyse verschiedener Kombinationen zielt diese Arbeit darauf ab, den Einfluss auf die Plankomplexität auf die reale Applizierbarkeit bei der Bestrahlung durch den LINAC zu bewerten und durch Variation dieser Parameter zu differenzieren. Hierfür werden 15 realitätsnahe Behandlungspläne – jeweils fünf für Prostata-, Brust- (Mamma) und Kopf- und Halstumoren (HNO) – analysiert und jeder Plan repetitiv optimiert. Der MCS wird berechnet, um die Auswirkungen der Optimierungsparameter auf die Plankomplexität zu bewerten. Zusätzlich werden Messungen an einem Phantom (Delta4+, Scanidos, SWE) vorgenommen, um die berechneten Kenngrößen der Pläne zu vergleichen beziehungsweise zu validieren. Die Ergebnisse der Arbeit tragen zu diesem Fachgebiet bei, indem sie ein klareres Verständnis dafür liefern, wie sich verschiedene Optimierungssparameter auf die Komplexität von realitätsnahen Strahlentherapieplänen und deren dosimetrische Applizierbarkeit auswirkt.

Acknowledgment

Finalising my Masters degree by finishing this Diploma thesis, a great journey comes to an end. So I want to use the next few sentences to mention everyone who encouraged and helped me, to achieve this work.

First of all, a special thanks to my thesis supervisor Professor Karin Poljanc, for inspiring me to get the most out off myself and lead me through this working process of this thesis. Her kindness and huge knowledge about this topic made it even possible for me to be there, where I am now.

Secondly, I would like to extend my deepest thanks to Dr. Christoph Gaisberger, who had the trust and faith to offer me the tremendous opportunity to work at the medical physics department in Salzburg. He guided me through every competition I had to face and teached me in the best way to become a medical physicist one day . Additionally I would like to extend my sincere thanks to the whole physicist team and informatics who always took their time for help and advises. Without all of their help and knowledge, I would not be able to set up this kind of project.

Finally i would like to thank my family and my closest friends for the tremendous support during this tough time during my study process. I could not be there without them.

Contents

Acronyms

Variable Name/Acronym	Description
Avg. LT	Average Leaf Travel
A/U	Aperature area divided by the circumference
TaG	Tangue and Groove
MCS	Modulation Complexity Score
MU/cGy	Monitor Units per centiGray
LTMCS	Leaf Travel multiplied by MCS
GS	Gantry Spacing
IT	Number of Iterations
γ	Gamma factor
LINAC	Linear Accelerator
TERMA	Total Energy Released per unit Mass
PSK	Point Spread Kernel
CC	Collapsed Cone
IMRT	Intesity Modulated Radiation Therapy
VMAT	Volumetric Modulated Arc Therapy
MLC	Multi-leaf Collimatior
MRI	Magnet Resonance Imaging
CT	Computer Tomography
PET	Positron Emission Tomography
DVH	Dose Volume Histogram
MU	Monitor Unit

Table 1: Acronyms and their meanings

1 Introduction

Scince the discovery of X-Ray radiation by Wilhelm Conrad Röntgen 1895, the evolving field of physics in medicine could no longer be imagined without it. So it didn't take long until it was recognized that this kind of radiation cannot only be used for medical imaging. Instead Physicists used it for a treatment method and tried to cure cancer cells. Therefore the first machines and methods were invented to create high energy radiation for a common cancer treatment therapy. [20]

Radiation therapy is one of the main methods in the treatment of various cancers worldwide. This medical invention uses high-energy particles or waves, such as X-rays, gamma rays, electron beams, or protons, to destroy or damage cancer cells. Among these, photon therapy, employing high-energy X-rays, is the most common form of radiation therapy. Generally, radiation therapy works by breaking the DNA within cancer cells, inhibiting their ability to reproduce and spread. [6] Photon therapy, in particular, X-rays - electromagnetic radiation with the ability to penetrate deep into the body, targeting tumors while sparing surrounding healthy tissue as best as possible. The precision and effectiveness of photon therapy have made it a fundamental component of cancer treatment methods, either as a standalone therapy or in combination with surgery or chemotherapy, or immunotherapy. [39]

In order to lead out a photon beam radiation therapy, an electron linear accelerator (LINAC) is used to produce fast electrons allowing these electrons to collide with a heavy metal target to produce X-rays. These X-rays are then shaped and directed to the patient's tumor, with precision control over their intensity. This capability not maximizes the dose to the tumor but also minimizes the exposure of surrounding healthy tissues and organs to radiation and also reducing side effects and improving patient outcomes. Generally the LINACs offer precision and flexibility in treatment delivery, allowing for the customization of radiation beams in many

dimensions like beam shaping and table adjustments. This is crucial in treating irregularly shaped or tumors that were usually challenging to target effectively. [18] Further, LINACs can be equipped with sophisticated imaging technologies, such as onboard CBCT (Cone beam computed tomography) scanning, enabling real-time imaging of the tumor before and during treatment. This feature, known as image-guided radiation therapy (IGRT), ensures that the radiation is delivered accurately to the tumor, accounting for any movement of the tumor or patient between sessions.

Moreover, the evolution of linear accelerators has given rise to advanced techniques such as intensity-modulated radiation therapy (IMRT) and volumetric modulated arc therapy (VMAT). These techniques allow for the modulation of the radiation dose intensity within each beam, offering a much faster dose delivery. The main goal of this work is to investigate some of the so called critical technical parameters of these LINAC's which influences the planning process and the therapy itself. Those parameters are for instance the gantry spacing, Multi-Leaf Collimator (MLC) characteristics, Modulation Complexity Score (MCS) and the Gamma index. All these parameters effecting the LINAC itself, lead to a specific plan complexity which then can be optimized for the best practical and clinical therapy. This also depends even on the therapy method, if either IMRT or VMAT is choosen.

1.1 Basics of photon radiation

Photon therapy is currently the most common radiation therapy method utilizing high-energy X-rays or gamma rays to treat various types of cancer. This specific approach uses the physical and biological properties of photons to deliver dose of radiation to a patients tissue. Photon therapy usually uses the high-energy photons generated by linear accelerators. These photon sources are either isotropic or non-isotropic and emit usually monoenergetic or heterogeneous photon beams. [19]

How does the photons get generated?

To generate photons that are practically useful for radiation therapy a well known procedure is used. The so called Röntgenstrahlung or X-rays emerge out of two different effects. The first is the so called characteristic x-rays.

1.1.1 Characteristic X-rays

The characteristic lines of the X-ray spectrum are produced by an interaction between an free electron colliding with a shell electron of an atom. If the energytransfer of this collision is higher than the boundary energy $E_n = -\frac{Z^2 R_H}{n^2}$ of a single electron in the shell, the electron gets emitted.

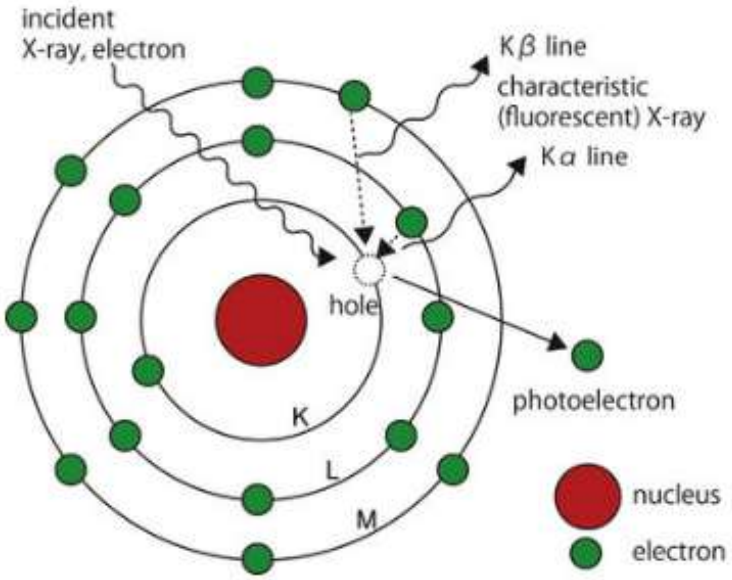

Figure 1.1: Characteristic X-rays emerging from an incident electron or photon. [42]

The resulting gap is closed by an electron from a shell either of a close shell or an outer shell. This can only be done, if the electron releases the energy difference during the step to fill the gap. This energy difference is emitted in the form of a photon. And, depending from which shell the electron comes, a characteristic peak in the energy spectrum can be seen.

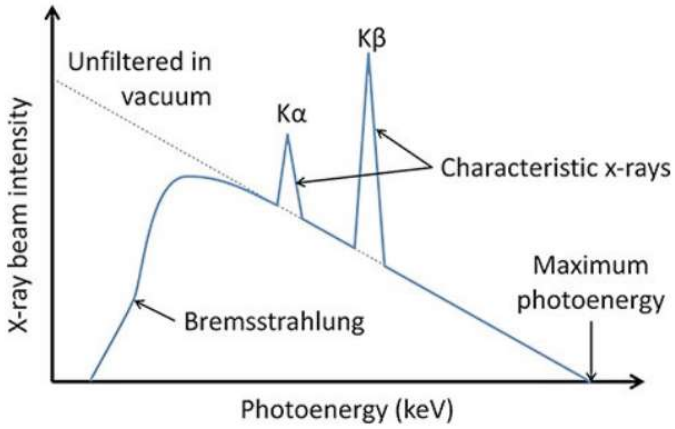

Figure 1.2: Xray spectrum with its characteristic lines. [47]

1.1.2 Bremsstrahlung

The second type of X-rays is the so called Bremsstrahlung. It is a continuous spectrum, in contrast to the discrete spectral lines, produced by the interaction of an incident electron with an atomic charge field of the nuclei. When a charged particle accelerates or decelerates, it emits electromagnetic radiation due to the change in its kinetic energy. For an electron interacting with a nucleus, this radiation is known as Bremsstrahlung. The energy of the emitted photon depends on the degree of deceleration and the electric field strength of the nucleus.

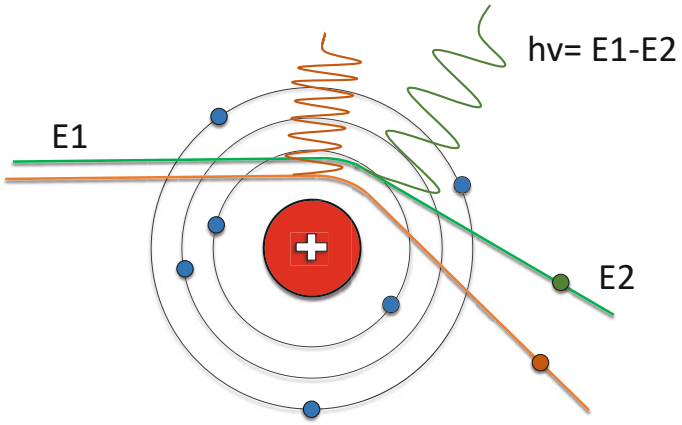

Figure 1.3: Bremsstrahlung at continous energy levels.

The intensity of the radiation $I(E)$ as a function of photon energy E can be described by:

$$I(E) = \frac{16}{3} \frac{Z^2 e^6}{m_e^2 c^4} \frac{1}{E} \ln\left(\frac{2E_{max}}{E}\right) \tag{1.1}$$

where:

- Z is the atomic number of the nucleus,
- e is the electron charge,
- m_e is the electron mass,
- c is the speed of light,

- E_{max} is the maximum energy of the electron.

This formula indicates that the intensity decreases with increasing photon energy and is more significant at lower energies.

Total Bremsstrahlung Power

The total power radiated due to Bremsstrahlung by an electron with energy E_e in a material with atomic number Z and electron density n_e is given by:

$$P = \frac{16}{3} \frac{Z^2 e^6 n_e E_e}{m_e^2 c^3} \tag{1.2}$$

This equation shows that the power emitted is proportional to the electron density and the energy of the incident electrons.

1.2 Mechanisms of Photon Interaction with Materials

Photon interactions with materials especially tissue are crucial in understanding various physical phenomena and applications, including medical imaging, radiation therapy, and materials analysis. There are three primary mechanisms of photon interaction with matter which all occur on different energies on the spectrum.

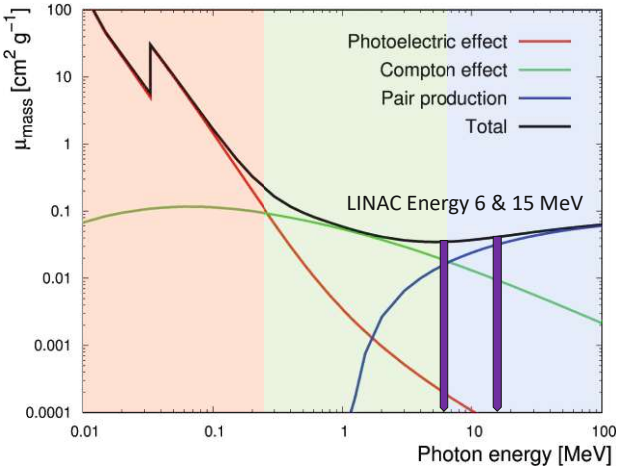

Figure 1.4: Primary mechanisms of photon interaction with matter and their Energy dependency.

1.2.1 Photoelectric absorption

Photoelectric absorption is a process in which an incident photon is completely absorbed by an atom, resulting in the ejection of an electron from one of the atom's inner shells. This interaction typically occurs at photon energies just above the binding energy of the electron in the shell. The ejected electron, known as a photoelectron, carries away the energy of the incident photon minus the binding energy of the electron.

$$E_{\mathrm{e}} = h\nu - E_{\mathrm{b}},$$

where E_{e} is the kinetic energy of the ejected electron, $h\nu$ is the energy of the incident photon, and E_{b} is the binding energy of the electron in the atom.

The probability of photoelectric absorption occurring is highly dependent on the atomic number (Z) of the absorbing material and the energy of the incident photon. Specifically, the cross-section for photoelectric absorption varies approximately as Z^3/E^3, where E is the photon energy. Therefore, materials with higher atomic numbers are more likely to exhibit photoelectric absorption, particularly at lower photon energies.

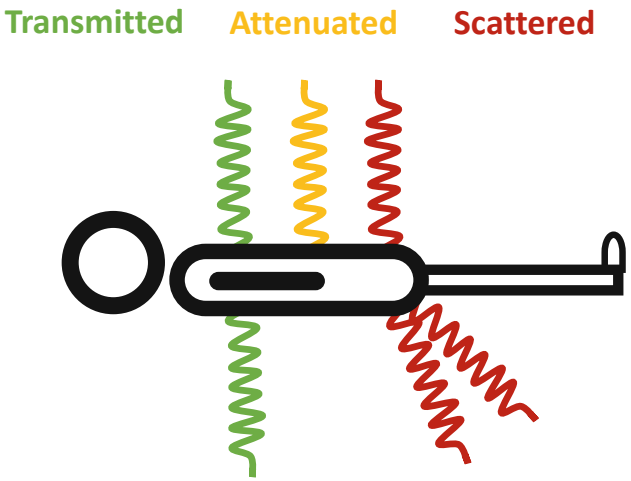

Figure 1.5: Photon interaction in the human body described with the Photoeffect and the Compton Scattering.

The photon radiation can either get transmitted, attenuated or scattered as in the picture seen above. These mechanisms are significant in applications such as X-ray imaging and radiation therapy. In X-ray imaging, photoelectric absorption

enhances the contrast between different tissues, as bones (high Z materials) absorb more X-rays compared to soft tissues. In radiation therapy, Compton scattering is highly relevant in the treatment planning, predicting the dose distribution in the specific area of the body. The energy deposit during the scattering process results in a complex calculation process.

1.2.2 Compton scattering

Compton scattering is another crucial interaction mechanism where an incident photon scatters off a loosely bound outer-shell electron. During this process, the photon transfers part of its energy to the electron, which is ejected from the atom, and the photon itself is deflected with reduced energy.

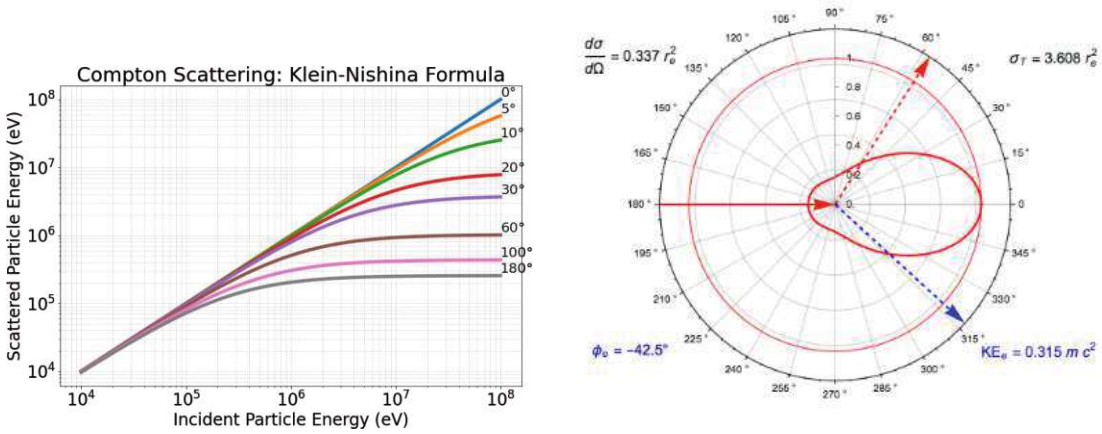

Figure 1.6: Compton Scattering diagram and Klein Nishina plot [36] for a specific cross section and angular.

The amount of energy transferred to the electron and the angle of photon deflection are described by the Compton equation and can be see in in th Fig[1.6] above:

$$\Delta\lambda = \frac{h}{m_e c}(1 - \cos\theta),$$

where $\Delta\lambda$ is the change in the photon's wavelength, h is Planck's constant, m_e is the electron rest mass, c is the speed of light, and θ is the scattering angle of the photon.

Compton scattering is relatively independent of the atomic number and is more probable at intermediate photon energies. The probability of an scattering photon

from a free shell electron can be described with the so called differential cross section $\frac{d\sigma}{d\Omega}$. The formula given for this differential equation is the Klein-Nishina formula, which is a key aspect of Compton scattering. This formula takes into account the relativistic effects of the electron and is given by [26]:

$$\frac{d\sigma}{d\Omega} = \frac{r_e^2}{2}\left(\frac{E'}{E}\right)^2\left(\frac{E'}{E} + \frac{E}{E'} - \sin^2\theta\right)$$

where:

- $\frac{d\sigma}{d\Omega}$ is the differential cross-section.
- r_e is the classical electron radius, given by $r_e = \frac{e^2}{4\pi\epsilon_0 m_e c^2}$.
- E is the energy of the incident photon.
- E' is the energy of the scattered photon.

The energies E and E' are related by:

$$E' = \frac{E}{1 + \frac{E}{m_e c^2}(1 - \cos\theta)}$$

Cross-Section

The cross-section is a measure of the probability of a scattering event. In the context of the Klein-Nishina formula, the total cross-section σ can be obtained by integrating the differential cross-section over all solid angles [36],[38]:

$$\sigma = \int \frac{d\sigma}{d\Omega}\, d\Omega$$

For the Klein-Nishina case, this integral takes into account the dependence of the cross-section on the scattering angle θ and the energies of the incident and scattered photons.

1.3 Radiation Dose Delivery

1.3.1 Radiation Dose Measurement and Units

Absorbed Dose (D)

The absorbed dose is a measure of the energy deposited by ionizing radiation per unit mass of tissue. It is a fundamental dosimetric quantity used in radiation therapy to quantify the amount of energy imparted to tissue from radiation. [27]

$$D = \frac{dE_{\text{abs}}}{dm}$$

- **Unit**: Gray (Gy), where 1 Gy = 1 Joule per kilogram (J/kg)
- **Usage**: Used to quantify the energy imparted to tissues and organs in patients undergoing radiation therapy.

Equivalent Dose (H)

The equivalent dose takes into account the type of radiation and its biological effect. It is calculated by multiplying the absorbed dose by a radiation weighting factor w_R specific to the type of radiation (e.g. photons have a lower value than protons or alpha particles). [27]

$$H = D \times w_R$$

- **Unit**: Sievert (Sv)
- **Usage**: Used in radiation protection to account for the different biological effects of various types of radiation.

Effective Dose (E)

The effective dose is a weighted sum of the equivalent doses in all tissues and organs, taking into account the varying sensitivities of different tissues to radiation. [27]

$$E = \sum_T w_T \times H_T$$

- **Unit**: Sievert (Sv)
- **Usage**: Used to assess the overall risk of radiation exposure, combining both the type of radiation and the tissues affected.

Kerma (K)

Kerma stands for Kinetic Energy Released in Medium and measures the initial kinetic energy transferred from photons to charged particles in a material. [27]

$$K = \frac{dE_{\text{tr}}}{dm}$$

- **Unit**: Gray (Gy)
- **Usage**: Used in the characterization of radiation beams, particularly in dosimetry for radiological protection and radiation therapy.

1.3.2 Dose Distribution and Tissue Response

The spatial distribution of the absorbed dose in a medium, especially in human tissue, is very important to understand, because the whole treatment process in radiation therapy is based on it to ensure that the target tissue receives the intended dose while minimizing exposure to surrounding healthy tissue. There are of course some differences in within the types of radiation which is used or tools such as collimators, wedges and filters to achieve the desired dose distribution. The calculated spatial distribution in the treatment planning system is the first look on and gives insights about which tissues gets which amount of dose or are the clinical goals fulfilled.

Dose Profile

The so called dose profiles represent the dose distribution across a plane perpendicular to the central axis of the radiation beam. They are essential for understanding the uniformity and symmetry of the radiation field which is delivered from the LINAC. Factors such as field size, distance from the source, and the use of beam modifiers can affect the dose profile. Usually there are two modes from the LINAC how the photon beam can escape the target. With or without a flattening filter to cover up

the high dose peak in the middle of the beam. These modes are optional an can be changed from treatment to treatment. In clinical practice, dose profiles help verify that the treatment plan conforms to the desired dose distribution and identify any potential hot or cold spots within the radiation field. [9]

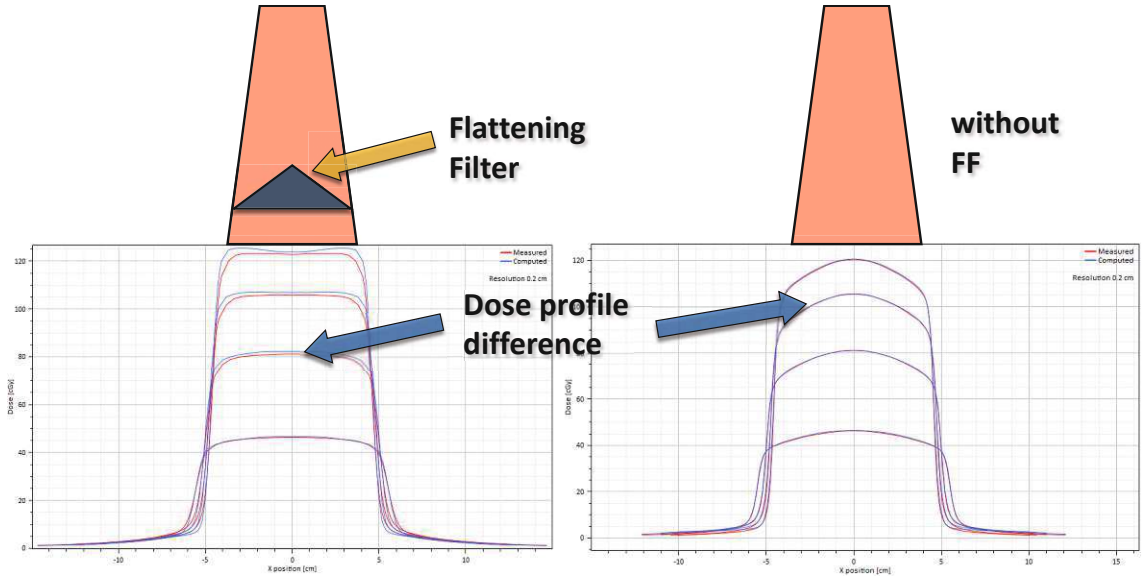

Figure 1.7: Dose profiles in different depths at 6MV with/without a flattening filter

Depth Dose Curves

Depth dose curves show the variation of dose with depth along the central axis of the radiation beam. These curves are essential for understanding how the dose is deposited within the body at different depths regarding to the effects discribed in the sections before. For a treatment planning these depthdoses will add up into the tumor region to ensure the right treatment. The curves are derived from measurements taken along the central axis of a radiation beam in a so called water phantom, which should simulate the human tissue for an exact dose build up inside the humand body. Furthermore its worth mentioning that depthdose curves are very different for photons or mass particles, which makes a tremendous contrast in the treatment therapy planing step.
The delivered dose gets measured in small steps into the depth, so the curve can be derived. A depthdose curve for different field sizes of photon beam of a LINAC can look like this:

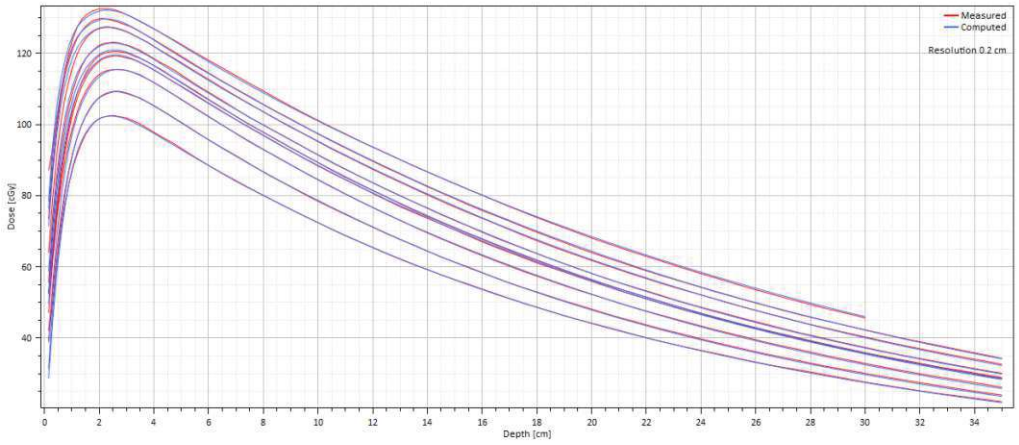

Figure 1.8: Depthdose profile of a 15MV beam for various field sizes

1.4 Treatment Planning in Radiation Therapy

The treatment planning process for radiation therapy begins in general with a consultation with a radiation oncologist. Therefore the best treatment technique will be evolved based on the current information of the specific cancer diagnosis. Every common treatment type e.g. radiotherapy can also be combined with the others, to get a much more sufficient result curing the cancer disease. Depending on the region where the malign tissue occurs, brachy- or tele radiotherapy might get chosen. In order to get the most precise treatment, a constant imaging of the desired region has do be done. The final step in order to confirm a treatable radiation plan is the quality assurance which has to be done to ensure an accurate plan and settings on the device. Therefore many parameters can vary and maybe has to be checked twice. [23],[5] This thesis is also part of the QA and validation process to improve the knowledge and behavior of these parameters. And finally based on these information the physician can confirm the treatment plan for the next following sessions.

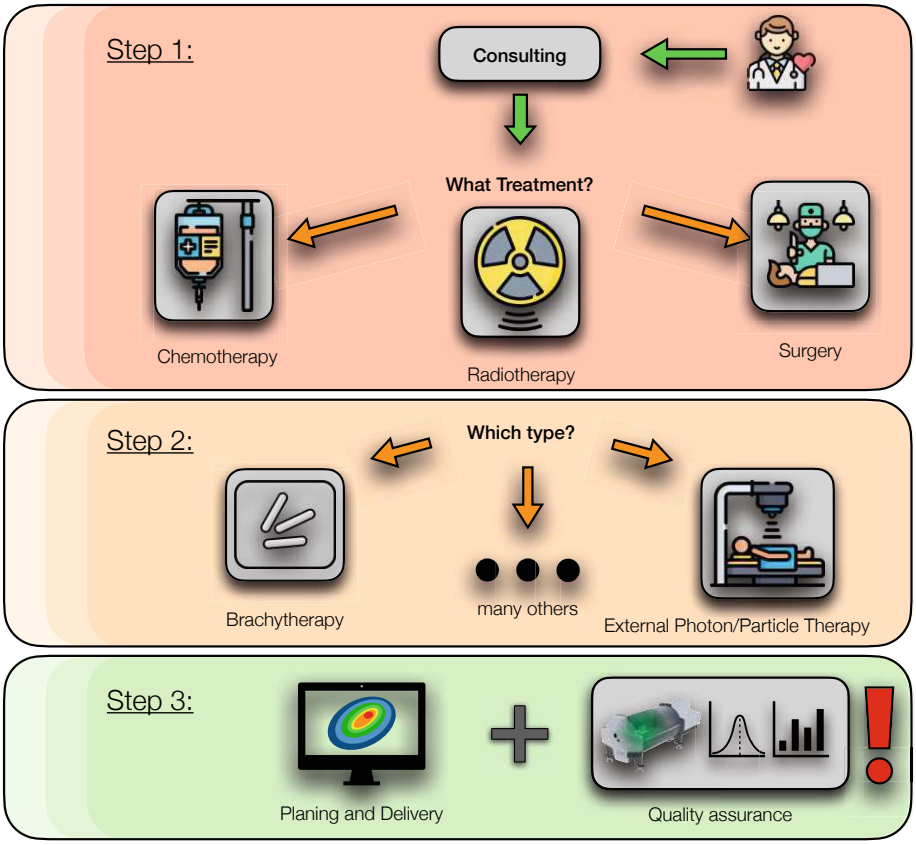

Figure 1.9: Important developing steps how to get the desired radiation therapy

1.5 Quality assurance and treatment validation

1.5.1 Importance of Quality Assurance

The Quality assurance process in radiotherapy is a critical process ensuring the safe and effective delivery of radiation to a patient. The complexity of modern radiotherapy techniques, such as IMRT and VMAT, requires specific methods and equipment like measuring phantoms or LINAC data and software to guarantee that the calculated dose is accurately delivered to the target while minimizing the dose to surrounding healthy tissues. [25] Furthermore the QA can also be a mechanism to improve the current state of radiation therapy and do a lot of research to keep the treatment at the highest step as possible.

The primary objectives of QA in radiotherapy include:

- Ensuring the accuracy of dose delivery according to the treatment plan.

- Minimizing the risk of treatment errors that could lead to underdosing the tumor or overdosing healthy tissues.
- Verifying the performance and calibration of treatment equipment, such as Linear Accelerators.
- Conducting patient-specific QA to validate that the planned treatment is executed as intended for each individual patient.

1.5.2 Monitoring Systems and Log Files for QA

Monitoring systems such as LINAC Watch (QUALIFORMED,GER/FRA) continuously track the performance of the linear accelerator in real-time, assessing parameters like beam output and gantry position to detect any deviations from the planned treatment. [33] This can be one method for a QA without directly measure the dose deviation on a specific tool. Additionally, log files from the LINAC and treatment planning system provide a detailed record of the treatment delivery process, allowing for retrospective analysis of any diversities between the planned and delivered dose distributions. [4] One specific device for monitoring dose delivery is the IQM (Integral Quality Monitor)(iRT Systems,Ger), a transmission detector mounted on the LINAC gantry that continuously measures the dose during patient treatment. The IQM's software continuously compares measured dose data with a reference dataset, enabling immediate detection of irradiation errors.

1.5.3 Measuring tools and Phantoms for dose validation

For dose distribution validation, phantoms such as the Octavius 4D (PTW, DE), ArcCHECK (Sun Nuclear Corporation, AUS), and Delta4+ HD (Scandidos, SWE) systems are commonly used. These systems differ primarily in their detector arrangement, which influences how they measure dose distributions. The Octavius phantom allows for broad patient-specific QA through its modular structure, containing planar dosimeters, typically arranged in a matrix, to measure dose distributions across different planes. [16] In contrast, ArcCHECK is specifically designed for rotational treatments like VMAT. It features a cylindrical design with a helical array of diodes arranged around the cylinder. This setup enables comprehensive measurement of dose distributions during arc therapy, providing full 360-degree coverage of

the treatment beam. [40] Similarly, the Delta4 phantom, developed by Scandidos, uses a 3D detector array, but the detectors are arranged in two perpendicular planes that intersect the treatment beam. This arrangement allows for high-resolution measurements in multiple dimensions, making it highly effective for QA in IMRT and VMAT.

Thus, the key difference between these systems lies in the arrangement of their detectors: the planar grid of Octavius, the helical diode array of ArcCHECK, and the 3D intersectional planes in Delta4. Each configuration is optimized for different treatment techniques, ensuring accurate dose distribution measurements.

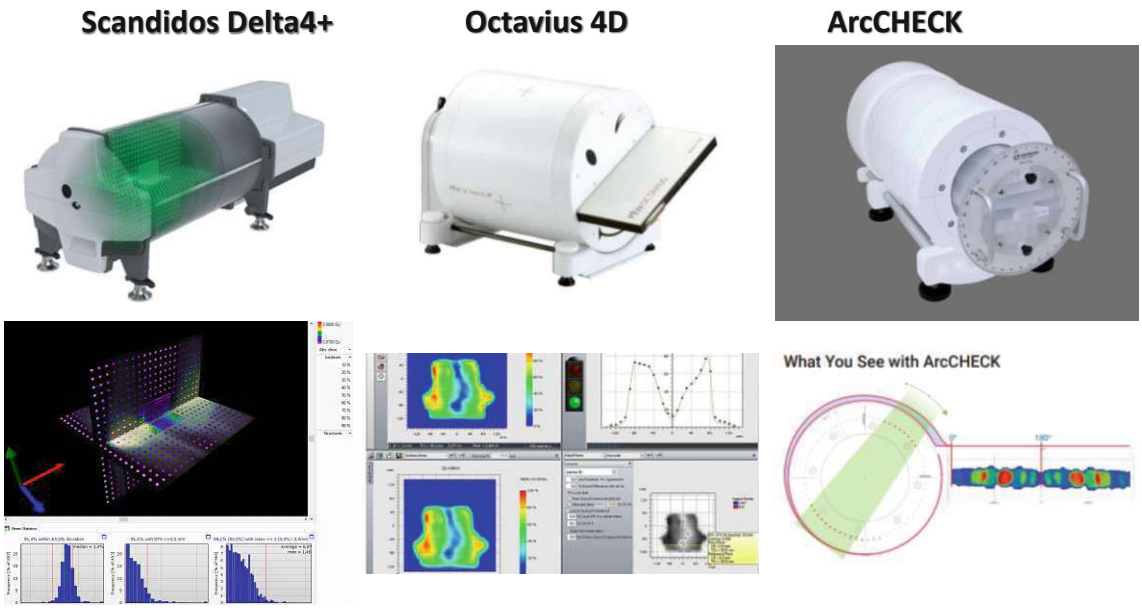

Figure 1.10: Different radiotherapy phantoms used for QA and dose validation ([3],[16],[40])

1.5.4 Need for Patient-Specific Validation

Patient-specific QA is a necessary component of the radiotherapy process because it accounts for the unique anatomical and treatment plan variations present in each individual case. Even when the treatment equipment is functioning within its specified tolerances, patient-specific factors such as anatomical heterogeneity, movement during treatment, and complex dose distributions have to be contained. This process ensures that:

- The treatment plan accurately accounts for patient-specific anatomy and positioning.
- The delivered dose conforms to the planned dose, despite the complexities introduced by patient anatomy and movement.
- Any potential errors in dose calculation or delivery are identified and corrected before treatment is administered.

By performing patient-specific validation, clinicians can provide a higher level of assurance that the treatment will be both safe and effective, ultimately leading to improved patient outcomes. [24]

1.6 Intensity-Modulated Radiation Therapy

Intensity-Modulated Radiation Therapy is a state-of-the-art cancer treatment method that allows for the radiation dose to be shaped very precisely to the contours of the tumor. By modulating the intensity of the radiation beams, IMRT can target the tumor with high doses of radiation while minimizing exposure to surrounding healthy tissues and organs. The LINAC is equipped with multileaf collimators to deliver precise radiation doses and protect the surrounding tissue for unnecessary dose. [41]

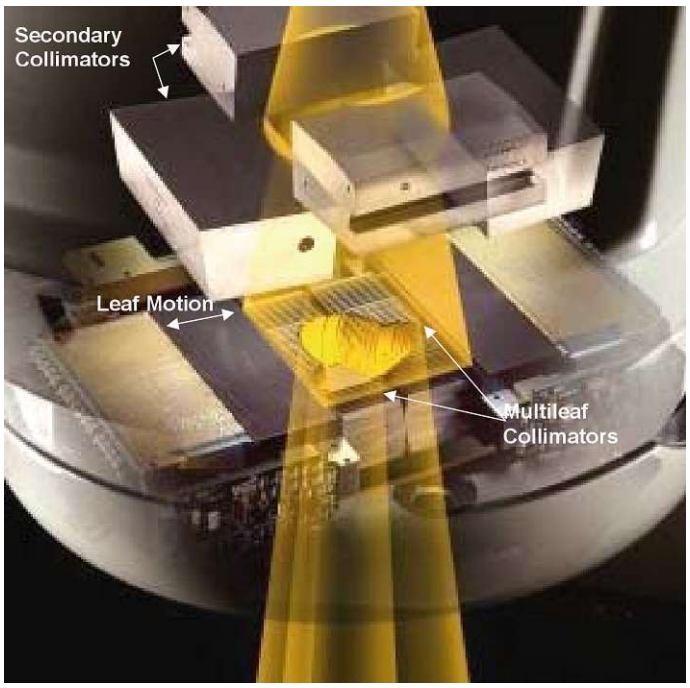

Figure 1.11: Insight photo of a LINAC seeing the MLC and how the leafs can be moved [15]

These leafs can be precisely moved (± 0.5 mm) in the desired position. The process of the treatment planning starts by claiming detailed imaging data, including the conventional imaging devices CT, MRI, or PET scans to develop a three-dimensional map of the target tissue. [21] The selling point of the IMRT tequniche is its ability to modulate the intensity of radiation beams across multiple small volumes within the tumor region. This modulation can be achieved through the single movement of the MLCs, which shape the radiation beams and adjust their intensity in real time for every calculated radiation field. Therefore different dose distributions are calculated for delivery to get a precise treatment of the target tissue. The dose finally adds up in the tumor and the healthy tissue can be protected as much as possible. [46]

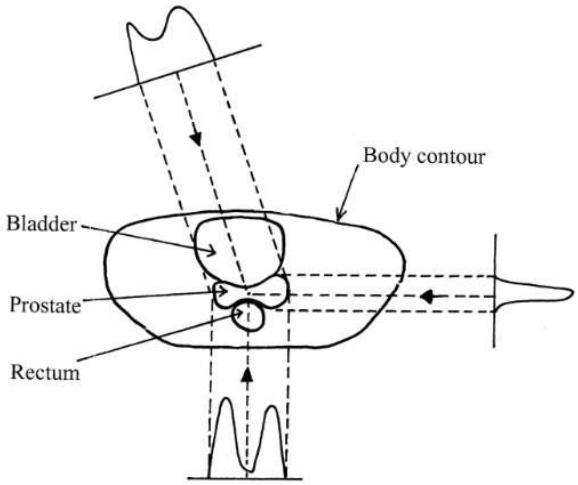

Figure 1.12: This is a concept picture of how a different dose distributions be delivered [44]

That is a huge advantage when it comes to radiation protection. It should be always taken into account that the healthy tissue should get as less as reasonable achievable dose. This precision and flexibility in dose distribution means that it can be used to treat tumors in complex locations or those close to critical structures with a reduced risk of side effects. This capability makes IMRT particularly valuable in the treatment of cancers of the brain, spine, prostate, head, and neck, among others. [44]

Figure 1.13: This figure shows the radiation pattern concept of an IMRT treatment [44]

When is IMRT Used?

IMRT is commonly used in situations where tumor suppression with minimal collateral damage is crucial. It's often recommended for:

- Tumors that are near or involve critical organs and structures, where traditional radiation therapy might pose a high risk of damage.
- Cancers that have irregular shapes or that vary in density, requiring customized dose distributions for effective treatment.
- Cases where a higher radiation dose is needed to treat the cancer effectively, which might be unsafe with other methods due to the risk to nearby healthy tissue.

1.7 Volumetric Intensity Modulated Arc Therapy

Volumetric Modulated Arc Therapy is an advanced form of intensity-modulated radiation therapy that delivers precise radiation doses to a specific area. VMAT optimizes the treatment by modulating the intensity of the radiation beam and the shape of the beam in multiple small segments. Simultaneously, the gantry of the linear accelerator rotates around the patient, allowing for the radiation dose to be delivered from different angles. This technique enables high doses to be focused on the tumor while minimizing the dose to the surrounding healthy tissues, thus reducing the potential for side effects. [46]

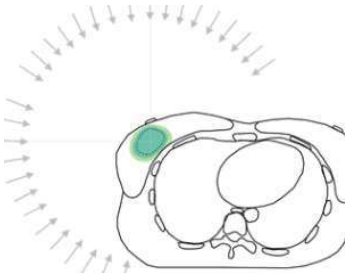

Figure 1.14: This figure shows the concept of a VMAT treatment. The pointers shows the rotations from the gantry of the LINAC [44]

The effectiveness of VMAT lies in its dynamic delivery. During treatment, the speed of the gantry rotation, the shape of the radiation beam, and the dose rate

are all varied. The beam is shaped by a multi-leaf collimator, which consists of numerous individual leaves that can move independently to block parts of the beam, thereby optimizing the beam shape and ensuring the protection of critical structures adjacent to the target volume.

One of the significant advantages of VMAT over conventional static field IMRT is the speed of delivery. A VMAT treatment can be completed in less time, often within a few minutes, making it more convenient for patients and potentially increasing the precision of the therapy, as there is less time for patient movement during treatment. VMAT has become a method of choice for treating a variety of cancers due to its accuracy, efficiency, and patient comfort, representing a significant advancement in radiotherapy technology.

However, there are also some disadvantages to consider:

- **Potential for inaccuracy**: Since the treatment is delivered in continuous arcs, it requires more precise control of the multi-leaf collimators (MLCs) and gantry. Any slight deviations during the rapid movement can introduce inaccuracies in dose delivery.
- **Increased interpolation**: VMAT relies heavily on the interpolation of dose between gantry positions, which may not always capture the full complexity of the dose distribution, especially in regions with steep dose gradients, leading to less accuracy compared to static field IMRT.
- **Longer calculation time**: The treatment planning process for VMAT is computationally more intensive, requiring complex algorithms to optimize dose delivery across multiple angles. This can lead to longer planning times compared to static IMRT.
- **Equipment stress**: The continuous motion of the gantry and MLCs during VMAT can put more mechanical stress on the treatment machine, potentially leading to more frequent wear and tear, increased maintenance, or reduced longevity of the equipment.

1.7.1 Multi-Leaf Collimators

Multi-Leaf Collimators are critical for shaping the radiation beam to conform to the tumor's geometry. MLCs consist of numerous individual leaves that can move independently to modulate the beam profile. This level of control allows for high conformity to the target volume, minimizes dose to surrounding healthy tissues, and enables sophisticated techniques such as Intensity-Modulated Radiation Therapy and Volumetric Modulated Arc Therapy.

The dose calculation must account for the MLC leaf positions, which impact both the primary radiation and the scatter components: [35]

Effects of MLC on Treatment

- **Beam Shaping:** The MLC allows for precise shaping of the radiation beam, enabling more targeted delivery of radiation. This can also be quantified as the area to circumference value which is also a crucial parameter considering the complexity of a plan.
- **Dose Distribution:** The configuration of the MLC can affect the dose distribution within the tumor and surrounding areas. Properly configured MLC settings can help ensure that the prescribed dose is delivered uniformly across the tumor.
- **Leaf Positioning Accuracy:** The accuracy of the leaf positions is crucial for treatment effectiveness. Any errors or uncertainties in leaf positioning can lead to suboptimal dose delivery, potentially impacting the treatment outcome.
- **Leaf Leakage:** While the leaves are designed to block radiation, there can be a small amount of leakage between the leaves. This can be characterized by the tongue and groovle value which is evaluated later on.

2 Project describtion

The primary aim of this project is to evaluate the modulation complexity at different key settings of Volumetric Modulated Arc Therapy plans using the Modulation Complexity Score and gamma index analysis. These metrics are critical in understanding the trade-off between achieving optimal dosimetric outcomes and ensuring precise treatment delivery in clinical settings.

The project investigates the impact of plan complexity on the deliverability and efficacy of treatment using a linear accelerator. It analyzes how various parameters, such as gantry spacing, dynamic behavior of the Multi-Leaf Collimator, and different optimization steps in the planning system, influence the quality and complexity of treatment plans. The project also explores how different these parameters adjust the quality assurance for a potential clinical application.

To achieve these objectives, 15 near realistic treatment plans are analyzed—five each for prostate, breast (mamma), and head and neck (ENT) tumors. Each plan undergoes multiple optimizations, with the MCS recalculated to assess the influence of these optimizations on plan complexity. Additionally, measurements are performed on a Delta4 Phantom+ (Scanidos, SWE) to validate the calculated parameters against actual dose distributions.

The project's outcomes are expected to contribute to a deeper understanding of how plan complexity affects treatment deliverability and to provide insights into optimizing radiotherapy plans for better patient outcomes.

3 Methods and Materials

3.1 Photon Dose Calculation

The Photon dose calculation is one of the most important section in an radiation planning treatment system. Either for clinical use or scientific measurements there are two main methods in the radiation planning system Raystation to calculate the photon dose in at a specific area in tissue or an other medium. The primary methods used are the Collapsed Cone Dose Computation and Monte Carlo Dose Computation. Each method has its unique approach to modeling the dose distribution within the patient. The process involves complex algorithms that consider the energy deposition of photons as they interact with tissues. [34]

3.1.1 Kernel based Algorithms

Kernel based algorithms use pre-calculated kernels and ray tracing to model dose deposition from interactions at specific points. These algorithms calculate dose by summing and scaling kernels according to the energy fluence at all points. Simple models like pencil beam utilize line kernels with ray tracing for fast dose computations. More complex models like convolution/superposition account for density variations and beam divergence, providing more accurate results but at a slower computation speed. [13]

What is a Kernel?

A kernel represents the energy spread resulting from an interaction at a specific point or line, caused by charged particles and scattered photons carrying energy away from the primary interaction site. Kernels, both line and point, are radially symmetric and pre-calculated using complex Monte Carlo simulations.

Ray Tracing

Ray tracing algorithms transport energy from the radiation source through the patient or phantom data set.

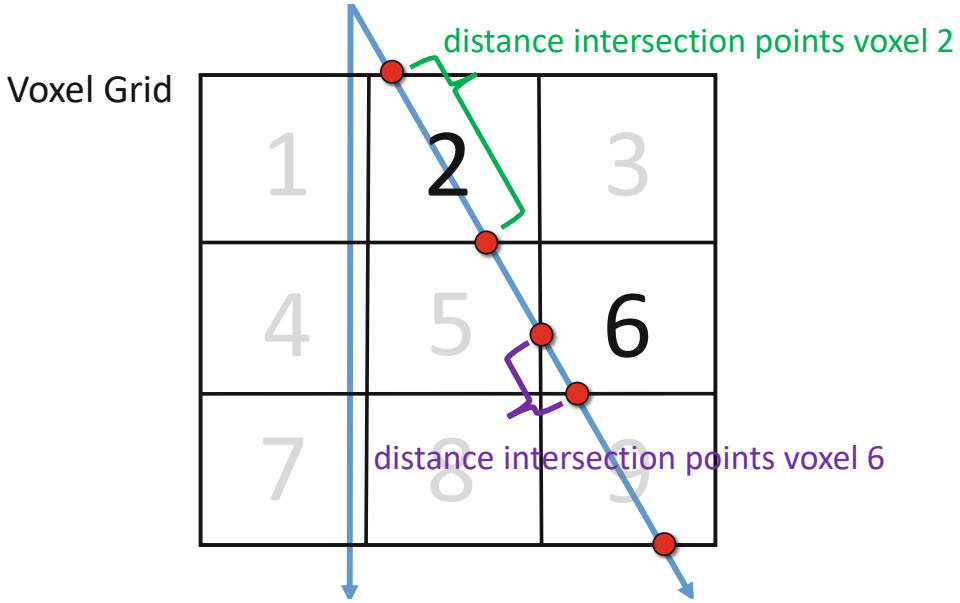

Figure 3.1: Simplified raytracing algorithm scheme

Steps in Ray Tracing

1. **Ray Generation**: A ray is projected from the radiation source through the aperture and into the patient data set.
2. **Intersection Points**: Points of intersection between the ray and voxel boundaries are identified.
3. **Distance Calculation**: The distance between intersection points within each voxel is computed.
4. **Fluence Scaling**: Fluence through the voxel is scaled based on the distance the ray travels through it.
5. **Ray Sampling**: Proper sampling of rays ensures a balance between calculation accuracy and computation time. Insufficient ray sampling can result in some voxels receiving no fluence.

In essence, kernel based algorithms leverage pre-calculated energy spread models and detailed ray tracing techniques to achieve accurate dose calculations in radiation therapy. [13]

3.1.2 Collapsed Cone Dose Computation

The Collapsed Cone (CC) dose computation method is one of the kernel based algorithms designed to efficiently model dose distribution by considering tissue heterogeneities and complex geometries. The slightly changed method compared to the pencil beam method, is focused on the separation between the three-dimensional transport of photons and the secondary electrons. [32] The dose distribution in a 3D volume is determined by a mathematical convolution of the energy released at different points (TERMA) as in Chapter [3.1.2] described, with how this energy spreads out (the kernel). This energy transfer is approximated using several tens of collapsed cones for each point where energy is released. Instead of considering every possible direction for energy spread, the method simplifies the problem by using these cones to represent the paths the energy takes. The dose is then calculated and summed only for the voxels that lie along the paths of these cones, rather than calculating the dose for every voxel in the volume. This approach makes the calculation more efficient while still capturing the essential distribution of the dose. [8]

The dose at a specific point r can be written as:

$$D(r) = \left(\frac{1}{\rho(r)}\right) \int\int\int\int TE(s)\rho(s)h(E, r', r)\, d^3s\, dE \tag{3.1}$$

To reshape it and express it in a more elegant way, we introduce the term $TERMA(r') = TE(r') \cdot \rho(r')$ and use $PSK(E, r', r) = h(E, r', r)$. The reshaped equation becomes:

$$D(r) = \left(\frac{1}{\rho(r)}\right) \int\int\int\int TERMA(r') \cdot PSK(E, r', r)\, d^3r'\, dE \tag{3.2}$$

Finally, we will see the convolution of the point-spread-kernel function and the TERMA:

$$D(\mathbf{r}) = \int TERMA(\mathbf{r}') \cdot PSK(\mathbf{r} - \mathbf{r}')\, d\mathbf{r}' \tag{3.3}$$

or short:

$$D(\mathbf{r}) = (TE * PSK)(\mathbf{r}) \tag{3.4}$$

So, in the reshaped equation, the integral over $\mathbf{r}'$ contains the integration over all spatial points within the medium, as well as the integration over all possible energy levels. [28] Both formulas represent the convolution of the TERMA with the PSK to calculate the dose distribution in the medium.

- $D(r)$ is the dose at point r.
- $\rho(r)$ is the density of the medium at point r.
- $TERMA(r')$ represents the Total Energy Released per unit Mass at point r'.
- $\rho(r')$ is the density of the medium at point r'.
- $PSK(E, r', r)$ is the Point Spread Kernel describing the distribution of dose around point s due to energy deposition at point r.
- The integral is performed over all space R^3 and over all energy levels from E_{min} to E_{max} to account for the spread of dose due to scattering and attenuation effects.

TERMA Computation

To calculate the photon dose, we need to introduce the so called TERMA. This stands for Total Energy Released per unit Mass and has properties of the medium at that location $\mathbf{r}'$. It represents the primary photon energy released in the medium and is depending on the energy fluence and the linear attenuation coefficient (μ).

$$TERMA = \Phi \cdot \mu$$

where Φ is the energy fluence. The linear attenuation coefficient accounts for the attenuation of primary photons and is integral to determining the energy deposition within the tissue.

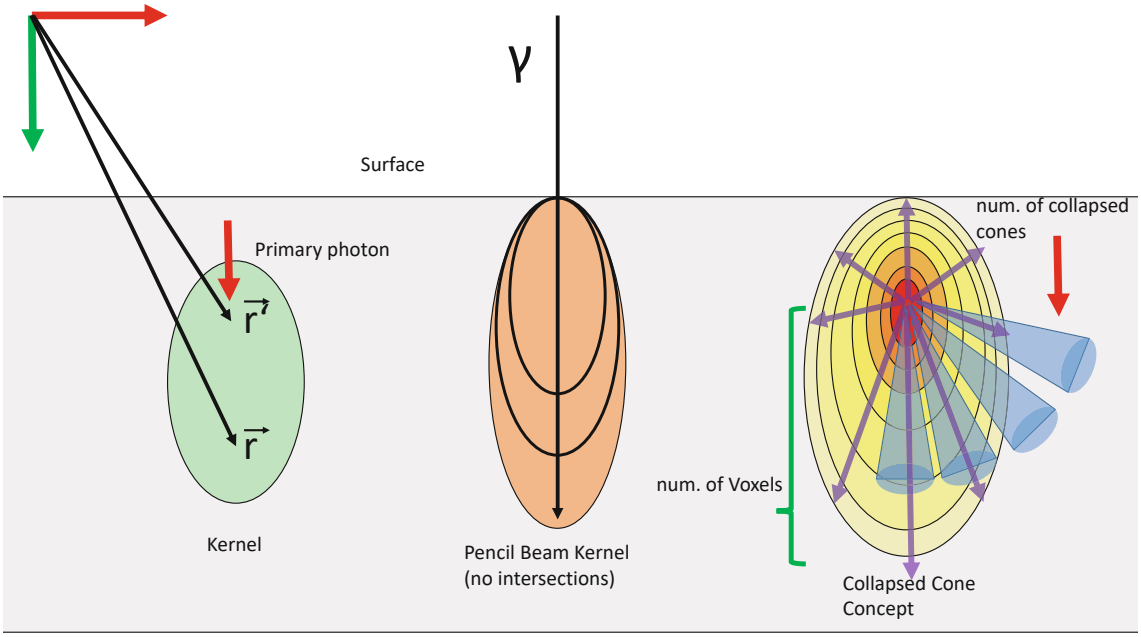

Figure 3.2: Visualizing the Collapsed Cone Concept vs. a single Pencil Beam Kernel

Linear Attenuation

The linear attenuation coefficient is a crusial parameter for calculating the photon dose especially, as mentioned before, the TERMA. It is an energy dependent parameter which represents the fraction of an X-ray beam that is absorbed or scattered. The coefficent can be derived through the interaction with a medium based on the photoelectric absorption. Chapter [1.2.1] and Compton scattering Chapter [1.2.2][26].

Derivation

$$dI = -\mu I \, ds$$

After integration, the familiar form is:

$$I = I_0 e^{-\mu s}$$

- I is the intensity of the X-ray beam after passing through a thickness s of the material.
- I_0 is the initial intensity.

- μ is the linear attenuation coefficient.

Energy Dependency

The linear attenuation coefficient is dependent on the energy of the X-ray photons and the properties of the material. It is expressed as the sum of the attenuation due to photoelectric effect $\mu_p(E)$ and Compton scattering $\mu_c(E)$[43]:

$$\mu(E) = \mu_p(E) + \mu_c(E)$$

Photoelectric Absorption

The photoelectric effect predominates at lower photon energies and its contribution to the attenuation coefficient can be approximated as:

$$\mu_p(E) \propto \frac{Z^m}{E^n}$$

Where:

- Z is the atomic number of the material.
- m and n are constants that depend on the energy range and material properties.

Compton Scattering

Compton scattering becomes significant at intermediate energies and its contribution is given by:

$$\mu_c(E) \propto \frac{Z}{A}$$

Where:

- A is the atomic mass of the material.

The combined expression for the linear attenuation coefficient [43], considering both photoelectric absorption and Compton scattering, is:

$$\mu(E) = a(E)\frac{\rho Z^m}{E^n} + b(E)\frac{\rho Z}{A}$$

- $a(E)$ and $b(E)$ are energy-dependent coefficients.

3.2 Modulation Complexity Score

The Modulation Complexity Score is a quantitative metric designed to assess the complexity of Intensity-Modulated Radiation Therapy treatment plans. The primary aim of the MCS is to evaluate how complex an IMRT plan is and predict its deliverability. High complexity in an IMRT plan often correlates with greater challenges in accurate dose delivery or longer treatment times. Understanding and calculating the MCS helps in balancing the trade-off between achieving dosimetric objectives and ensuring accurate, reliable treatment delivery. [30]

3.2.1 Definition of MCS

MCS is defined on a scale from 0 to 1.0, where a score of 1.0 represents a plan of zero complexity, such as an open rectangular field, and decreasing values indicate increasing complexity. The calculation of MCS involves two key parameters derived from the treatment planning system: the Leaf Sequence Variability (LSV) and the Aperture Area Variability (AAV). These parameters incorporate variations in leaf positions, the irregularity of field shapes, and segment weights into a single score. [30]

Leaf Sequence Variability

The LSV parameter quantifies the variability in the position of MLC leaves between adjacent segments. The LSV for each segment is computed using the following formula:

$$LSV_{\text{seg.}} = \left(\frac{\sum_{n=1}^{N} \left(\text{pos}_{\max} - |\text{pos}_n - \text{pos}_{n+1}| \right)}{N \cdot \text{pos}_{\max}} \right)_{\text{LB}} \times \left(\frac{\sum_{n=1}^{N} \left(\text{pos}_{\max} - |\text{pos}_n - \text{pos}_{n+1}| \right)}{N \cdot \text{pos}_{\max}} \right)_{\text{RB}} \tag{3.5}$$

where N is the number of open leaves, and pos_n represents the position of the n^{th} leaf.

Aperture Area Variability

The AAV parameter measures the variation in segment areas relative to the maximum possible aperture defined by all segments in the beam. The formula for AAV

is:

$$AAV_{\text{segment}} = \frac{\sum_{a=1}^{A} \left(\text{pos}_{a,\text{left bank}} - \text{pos}_{a,\text{right bank}}\right)}{\sum_{a=1}^{A} \left(\max(\text{pos}_{a,\text{left bank}}) - \max(\text{pos}_{a,\text{right bank}})\right)_{\text{beam}}} \tag{3.6}$$

where A is the number of leaves in the leaf bank.

Combining LSV and AAV into MCS

The final MCS for a beam incorporates LSV and AAV, weighted by the relative monitor units (MU) of each segment:

$$MCS_{\text{beam}} = \sum_{i=1}^{I} \left(AAV_{\text{segment},i} \cdot LSV_{\text{segment},i} \cdot \frac{MU_{\text{segment},i}}{MU_{\text{beam}}} \right) \tag{3.7}$$

where I is the number of segments in the beam.

3.2.2 Overall Plan Complexity

The overall complexity of an IMRT plan, MCS_{plan}, is the weighted average of the beam MCS values:

$$MCS_{\text{plan}} = \sum_{j=1}^{J} \left(MCS_{\text{beam},j} \cdot \frac{MU_{\text{beam},j}}{MU_{\text{plan}}} \right) \tag{3.8}$$

where J is the number of beams in the plan. [30]

Calculation and Evaluation

The calculation of MCS involves extracting the required parameters (leaf positions, segment weights, etc.) from the treatment planning system. This score can then be used to evaluate and compare the complexity of different IMRT plans, facilitating decisions during treatment planning and quality assurance processes.

3.2.3 Predicting Plan Deliverability

Higher MCS values generally correlate with simpler, more deliverable plans. Conversely, lower MCS values indicate increased complexity, which can lead to greater challenges in accurate dose delivery. Therefore, MCS can serve as a predictive tool

for plan deliverability, potentially reducing the need for extensive patient-specific QA measurements by identifying plans that are likely to be robust in delivery.

3.3 MCS in VMAT

The complexity of a VMAT plan has nearly the same definition as in IMRT. It can be assessed using a modified version of the Modulation Complexity Score, adapted for VMAT, known as MCSv. [29] Therefore slight changes in the calculations has to be done and more informations about the single leaf travel has to be gained.

3.3.1 Definition and Calculation of MCS in VMAT

The MCSv, or Modulation Complexity Score for VMAT, is similar to the usual MCS value and just has slight differences in computation but with the same basic priciple. The MCSv extends the original MCS concept, [30] which was developed for step-and-shoot IMRT, to the continuous delivery of VMAT by considering the control points (CP) of the arc. [29]

The detailed components of MCS, such as Leaf Sequence Variability and Aperture Area Variability, described in Chapter [3.2.1], are adapted for VMAT planning. Here, we summarize the specific adjustments for VMAT:

Leaf Sequence Variability

For each control point in the arc, LSV is calculated the same way as in the section described before. The visualization below makes it more clear what is ment for the pos_{max}. It is the maximum distance from a leaf position for a specific leaf bank summed over all segments and beams in the given plan.

Aperture Area Variability

AAV for VMAT is computed by considering the area defined by the opposing leaves at each control point, normalized to the maximum aperture area over all control points in the arc. The area of a specific control point can look a bit like in the following schematic figure which illustrates a specific arrangement of the leafs during a VMAT treatment.

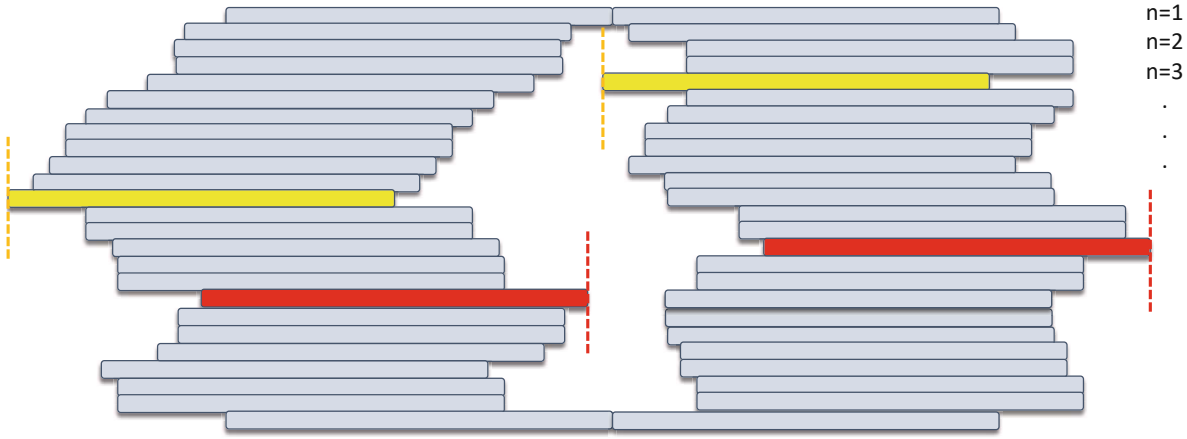

Figure 3.3: Schematic figure of visualizing how the LSV can be calculated

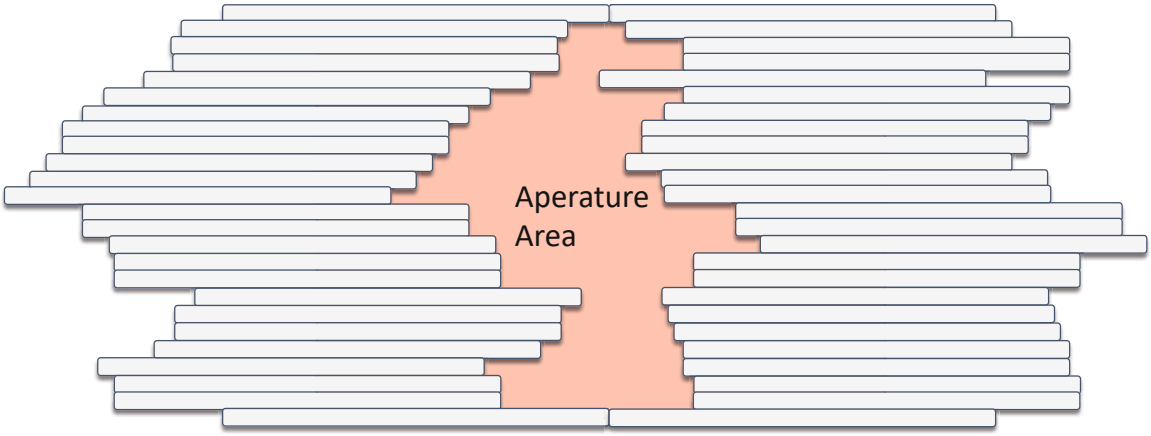

Figure 3.4: Schematic figure of visualizing how the AAV can be calculated

Combining LSV and AAV into MCSv

The MCSv for a VMAT arc incorporates LSV and AAV across all control points, weighted by the monitor units (MU) delivered between each pair of control points:

$$\mathrm{MCSv}_{\mathrm{arc}} = \sum_{i=1}^{I-1} \left(\frac{\mathrm{AAV}_{\mathrm{CP},i} + \mathrm{AAV}_{\mathrm{CP},i+1}}{2} \cdot \frac{\mathrm{LSV}_{\mathrm{CP},i} + \mathrm{LSV}_{\mathrm{CP},i+1}}{2} \cdot \frac{\mathrm{MU}_{\mathrm{CP},i,i+1}}{\mathrm{MU}_{\mathrm{arc}}} \right) \tag{3.9}$$

where I is the number of control points in the arc, and $\mathrm{MU}_{\mathrm{CP},i,i+1}$ represents the MUs delivered between control points i and $i+1$.

Predicting Dosimetric Accuracy

In VMAT planning, higher MCSv values generally correlate with simpler, more deliverable plans. Plans with lower MCSv values indicate increased complexity, potentially leading to greater challenges in accurate dose delivery. This correlation was observed in the study [29], where significant correlations were found between MCSv and gamma passing rates, indicating dosimetric accuracy.

3.3.2 Optimizing VMAT Plans

Understanding the MCSv allows clinicians to optimize VMAT plans by balancing dosimetric quality and complexity. For instance, plans with high leaf travel and complex modulation might require finer control point spacing to ensure accurate dose delivery. Masi et al. [29] demonstrated that reducing control point separation from 4° to 3° or 2° significantly improved the gamma passing rates, particularly for plans with high leaf travel values.

3.4 Gamma Index

The Gamma Index is a specific metric in radiation therapy which is commonly used in terms of Intensity-Modulated Radiation Therapy and Volumetric Modulated Arc Therapy. This parameter gives insight to the correlation between the measured and calculated dose distribution for a specific treatment plan which can be very import for patient-specific quality assurance.

3.4.1 Definition and Calculation

The calculation and evaluation of the Gamma Index are based on the paper by Daniel A. Low [10] and M. Hussein [22] but is summarized here for clarity. The Gamma Index integrates dose differences and distance-to-agreement (DTA) criteria into a singular metric, defined for a point in the evaluated dose distribution. It is based on finding the minimum Euclidean distance for each reference point derived by the following formula:

$$\gamma = \sqrt{\left(\frac{\Delta d}{DTA}\right)^2 + \left(\frac{\Delta D}{DD}\right)^2} \tag{3.10}$$

where:

- Δd represents the spatial discrepancy between the evaluated point and its counterpart in the planned dose distribution.
- DTA is the predefined maximum acceptable distance-to-agreement.
- ΔD denotes the dose deviation between the evaluated dose at a point and the planned dose at the corresponding point.
- DD is the predefined maximum acceptable dose difference.

To compute the Gamma Index for a particular point, an algorithm searches for the minimum value of γ by evaluating all possible points in the evaluated dose distribution. This involves calculating the Euclidean distance between the reference and evaluated points and the corresponding dose differences. A fast algorithm to calculate the Gamma Index was published by Markus Wendling [45] and the key points are summarized here for better understanding.

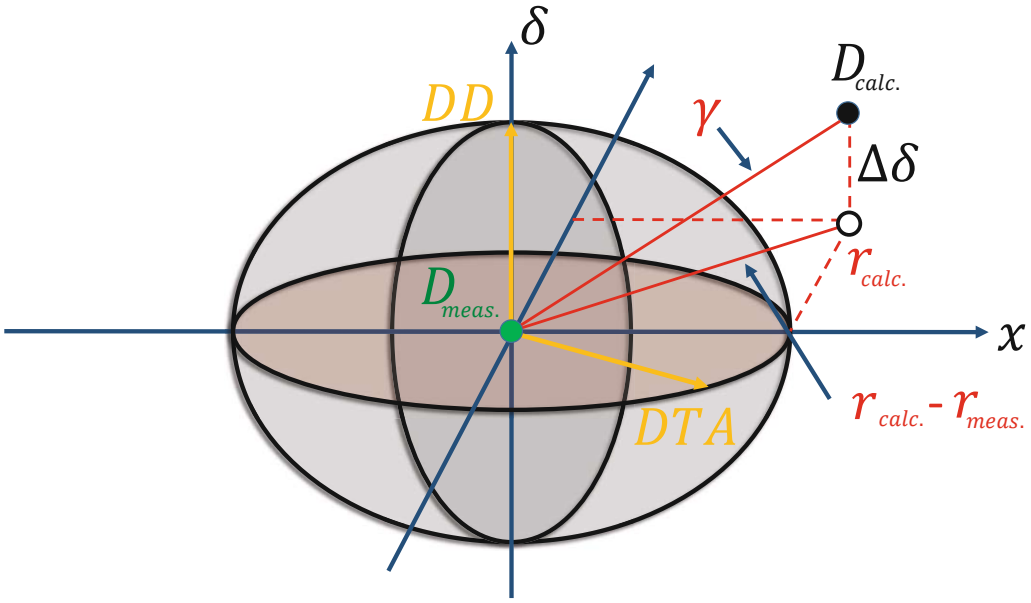

Figure 3.5: Geometric representation of the calculation of the Gamma Index using the Euclidean distance

1. Resampling of dose distribution for both, reference and evaluated dose at the same grid.

2. Definition of the dose difference and spatial distance.

3. Gamma index calculation (as mentioned before).

4. Calculate $\gamma_{(calc.)}$ for every reference point r by searching searching through $D_{(meas)}$.

5. Starting where $r_{(calc.)} = r_{(meas.)}$ and search around a sphere with radius of DTA for every reference point.

Interpretation

- A Gamma Index value of 1 or below signifies that the evaluated dose point meets or is within the set criteria of dose difference and distance-to-agreement compared to the planned dose distribution.
- Values exceeding 1 indicate discrepancies, pointing out that the point fails to adhere to the specified criteria, thus highlighting areas of non-conformance between the planned and delivered doses.
- Clinically, the Gamma Index pass rate, which quantifies the percentage of points with $\gamma \leq 1$, is often used to gauge the overall congruence. Acceptance thresholds commonly exceed 95% or 90%, although specific criteria may vary depending on the treatment complexity and institutional standards. [22]

3.4.1 The Correlation Between Plan Complexity and the Gamma Index in VMAT

Intensity-modulated radiation therapy and volumetric modulated arc therapy have significantly advanced the precision of radiation dose delivery to tumors while sparing adjacent healthy tissues. The development of these techniques has necessitated the evolution of comprehensive quality assurance measures to ensure the accurate execution of complex treatment plans. [23],[5] This thesis will further investigate the correlation between the complexity of VMAT plans and their verification through the Gamma Index, utilizing the ScandiDos Delta 4+ system for patient-specific QA.

3.4.2 Global and Local Gamma Index

The γ calculations can be evaluated either locally or globally. In the local test, the dose deviation is determined for each individual dose point of the reference distribution. For a global evaluation, the dose difference changes to:

$$\delta(r, r') = \frac{D_e(r') - D_r(r)}{D_{\text{norm}}}$$

The normalization dose D_{norm} can be defined differently, e.g., as the maximum dose within the reference dose distribution $D_r(r)$ or as a point in high-dose regions with a small gradient, resulting in a constant, absolute accepted measurement deviation for all points of the measured dose distribution. [22]

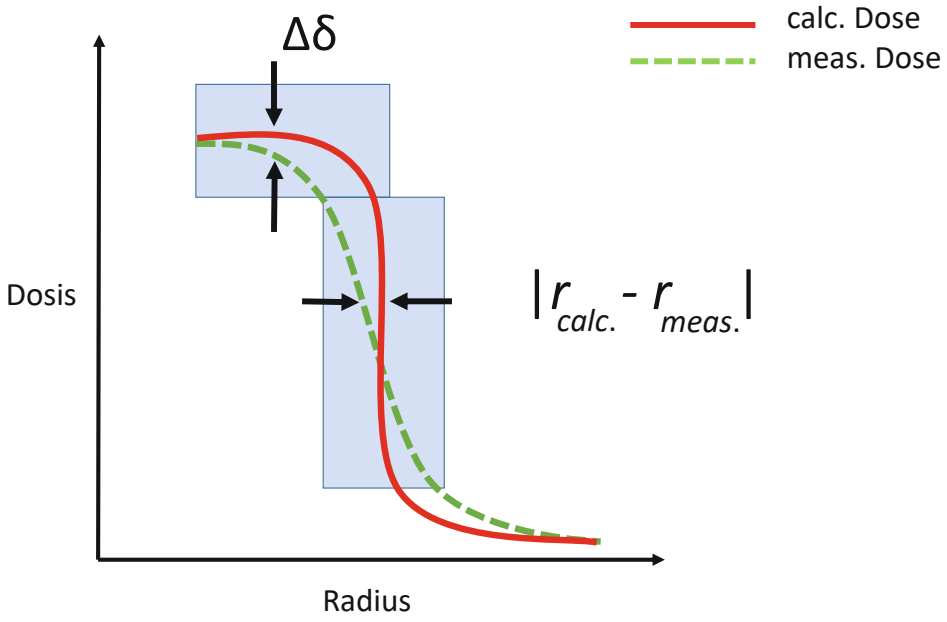

Figure 3.6: Schematic representation of the impact of global and local DD criteria on a 1D dose profile. While the gamma criterion ΔD_M for local DD applies to each reference point r, it remains constant for global DD through normalization. [12]

The local test (γ_{local}) tends to highlight inconsistencies between calculated and measured dose distributions in regions with high dose gradients and in low dose regions, while the global test (γ_{global}) tends to highlight inconsistencies in regions with higher doses within the dose distribution. Therefore, the local calculation is more suitable for a critical plan verification, as it particularly includes deviations in the low-dose area, where, for example, risk organs may be located, in the plan evaluation. Overall, the choice of the local or global calculation method depends on the internal requirements for the verification method. For interpreting the results, it is crucial to know which method was applied. If the global index is chosen, the selection of the normalization dose is equally crucial.

3.5 Gantryspacing

Gantry spacing is a critical parameter in the delivery of radiation therapy using linear accelerators, particularly in Volumetric Modulated Arc Therapy. It refers to the angular distance between the control checkpoints during the gantry's rotation around the patient. The choice of gantry spacing affects many other parameters of the LINAC and the characteristics of the generated treatment plan as we will see in this study.

Smaller gantry spacing, such as 2°, allows for more precise control over the dose distribution, as it provides a greater number of angles from which radiation can be delivered. This can result in improved conformality to the target volume and can potentially lead to better sparing of surrounding healthy tissues. However, this increased precision comes at the cost of longer computation times and increased complexity in terms of some crucial LINAC parameters. Conversely, larger gantry spacing, such as 4°, reduces the number of control points and can simplify the treatment plan, leading to faster delivery times. This may compromise the conformality of the dose distribution, particularly for targets with complex shapes or when critical organs at risk are in close range. But either high or lower gantry spacing the accuracy and mostly everything else also depends on the leaf motion speed too. [31]

The choice of gantry spacing is therefore a trade-off between the desired precision of the traveling leafes and the practical constraints of treatment time and planning complexity. Clinicians must consider these factors when selecting gantry spacing for

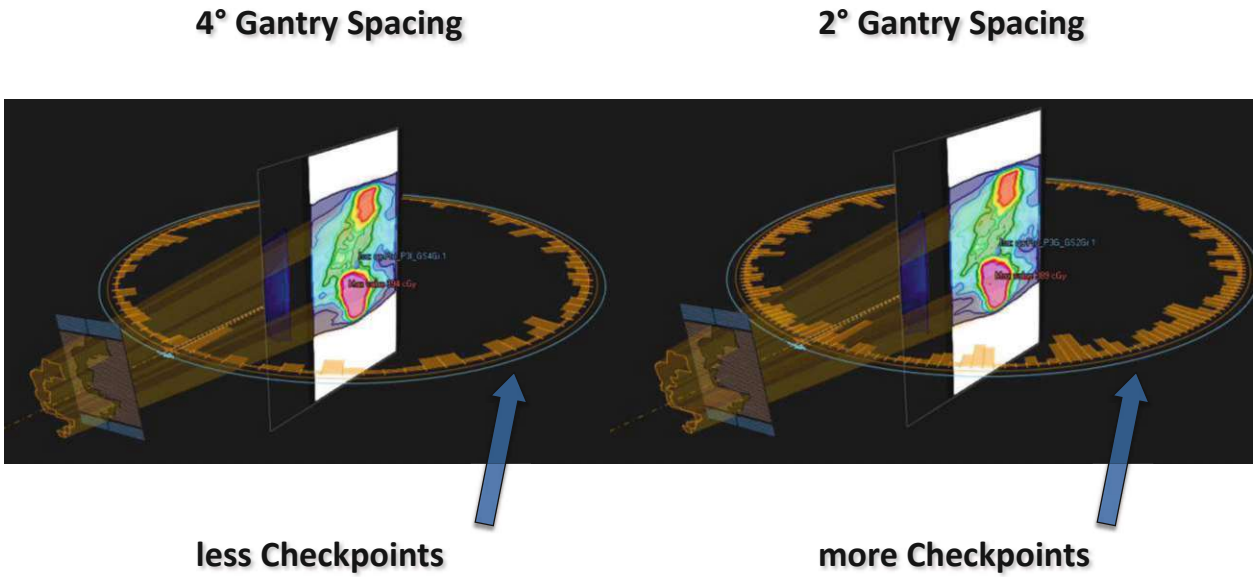

Figure 3.7: Gantry spacing 4°(less Checkpoints) vs 2°(more Checkpoints) [34]

a particular treatment plan.

RayStation, a leading treatment planning system, optimizes VMAT plans by considering these trade-offs in its algorithmic approach with the so called objective functions. The optimization process begins with the generation of initial fluence maps at key gantry angles. These maps are optimized to ensure that the dose distribution conforms to the target while minimizing exposure to surrounding healthy tissues. During the sequencing phase, these optimized fluence maps are converted into control points, which are then distributed over the entire arc. The control points are refined to achieve the desired gantry spacing, balancing the number of points against the need for precise dose delivery. [2]

RayStation employs a sorting algorithm that determines the optimal distribution of control points, minimizing leaf travel and ensuring compliance with machine constraints such as maximum leaf speed and valid dose rates. This allows for the efficient delivery of treatment plans with the desired gantry spacing, whether 2°, 3°, or 4°, while maintaining high precision and minimizing treatment time.

The optimization process in RayStation also involves simultaneous consideration of multiple arcs, which can further enhance dose distribution by providing additional

angles of delivery. This is particularly beneficial when dealing with targets that are close to critical organs at risk, as it allows for more precise control of the dose distribution.

In conclusion, gantry spacing is a vital impacting the precision, efficiency, and effectiveness of radiation therapy. RayStation's sophisticated optimization algorithms enable clinicians to tailor gantry spacing to the specific needs of each patient, ensuring optimal treatment outcomes.

3.6 Modulation

RayStation optimizes VMAT treatment plans by iteratively adjusting control points to achieve the desired dose distribution. The optimization process involves several key steps and considerations, aiming to balance the trade-offs between target coverage and organ-at-risk with many optimization functions which all have different objectives and constrains.

Optimization

The optimization begins with an initial guess of the objective function based on the clinical goals, such as target coverage and OAR sparing. RayStation uses various objective functions, including uniform dose, max dose, min dose, and DVH functions, to guide the optimization process. The objective function defines the desired dose levels and penalizes deviations from these levels. The calculated dose and the starting initial guess are based on the dose calculation algorithms mentions before. [1]Chapter:[3.1.2]&[3.1.1]
The objective value is a measure of how well the current dose distribution meets the defined clinical goals. It is calculated by evaluating the weighted sum of all objective functions. A lower objective value indicates a dose distribution closer to the desired outcome. During the optimization, RayStation iteratively adjusts the control points to minimize the objective value, improving the conformity and homogeneity of the dose distribution. [1] The visualization of the objective value by each iteration step in RayStation can be seen below.

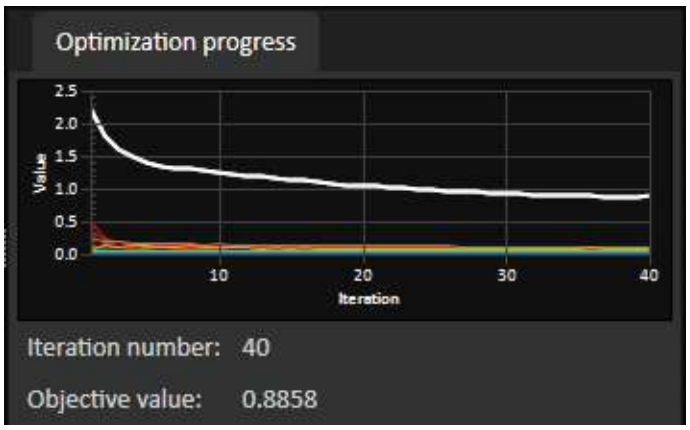

Figure 3.8: Objective value progress with each iteration step

The optimization process in RayStation is iterative. With each iteration, the system adjusts the control points to better meet the objective function. As the number of iterations increases, the objective value typically decreases, indicating an improved dose distribution. However, the rate of improvement may slow down as the optimization approaches convergence. The maximum number of iterations and the optimality tolerance are key parameters that influence the optimization process. The optimality tolerance determines the stopping criterion for the optimization. If the change in the objective value between iterations falls below this threshold, the optimization is considered to have converged. [1]

3.7 Measurement

The measurements were divided into two distinct sections, both performed on the same LINAC (Elekta Versa HD, SWE)[14] under similar conditions. These two sections were performed over several days, with each session started by a reference measurement. Before starting each cycle, the Phantom was placed as precise as possible in the isocenter of the LINAC with a guiding laser system. The correct placement of the phantom can be proven with a usual reference measurement, taken before the actual event. This reference measurement involved four static 10 cm x 10 cm^2 fields at 90-degree intervals, each delivering 100 Monitor Units. The build up of the measurement for the different gantry spacing levels and highly modulated plans was exactly the same and are illustrated in the picture below. The reference measurements had been done to ensure precise isocenter alignment of the phan-

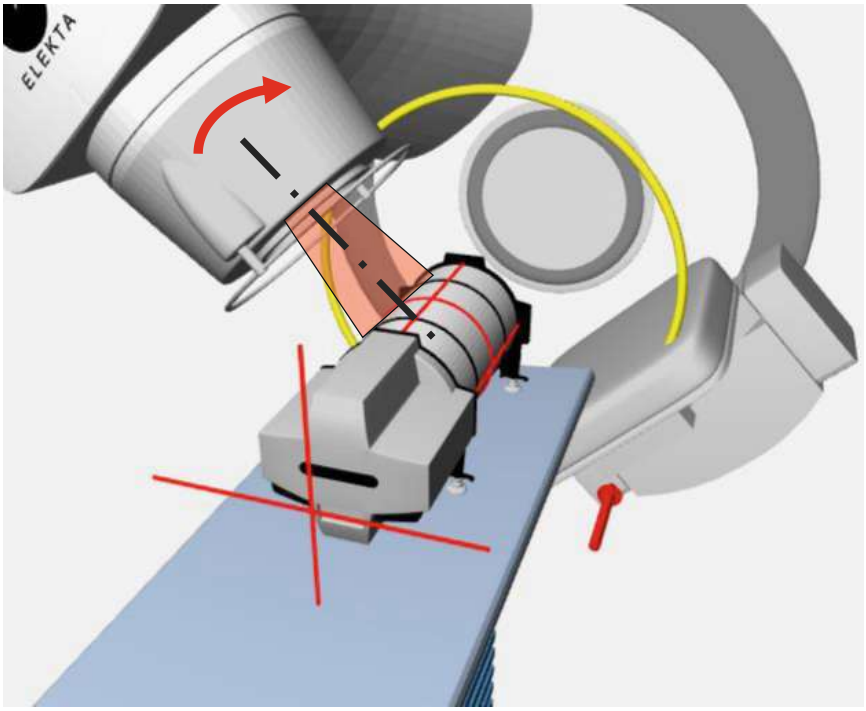

Figure 3.9: LINAC and Delta4+ showing how a radiation measurement can be done

tom and to assess the accuracy of the measured dose distribution compared to the planned dose. By analyzing these reference measurements, a correction factor can be calculated to normalize each measurement section from different days, enabling consistent and comparable results across all sessions.

3.8 Reference measurement

Before measuring straight up the gamma passing rates of the prepared plans, a reference measurement has to be done in order do guarantee a precise placement in the isocenter of the Delta4+ phantom. Regarding to the distance to agreement, a very small error range is crucial to get good results. Therefore a closer look at the planned and measured dose deviation in the important part of the beam has to be taken, to ensure such a perfect quality and settings for the upcoming measurements. The dose deviation curves of the reference measurement shows first of all that the phantom must be placed very precisely in the isocenter. The relative dose deviation is around 0.5 to 1%. In the center of the radiation field a perfect match between the planned and the measured dose can be seen.

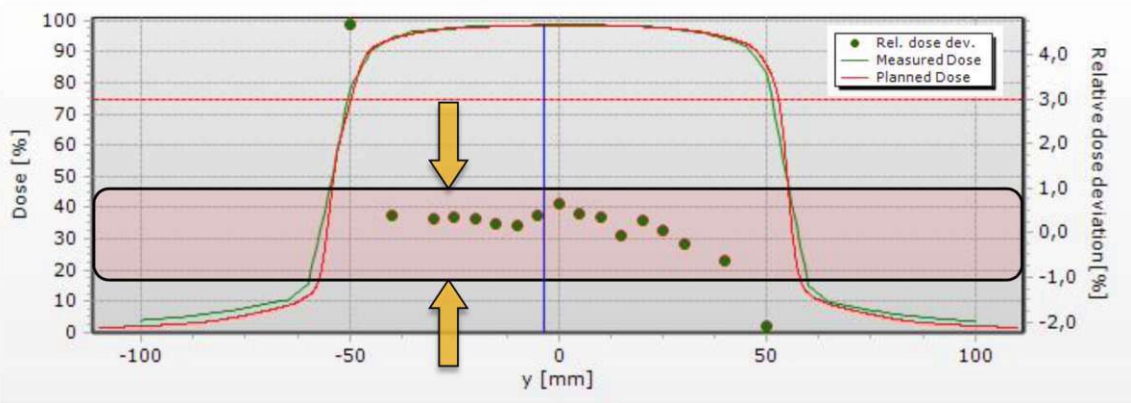

Figure 3.10: Dose deviation of the reference measurement

This has also been attributed by applying a temperature correction value to reshift an overdose in the measurement as described in the temperature dependency section of the Delta4+ Chapter: [3.9.2]. On the axis views it has still to be mentioned that slight overdose at the edged of the 10x10 cm^2 field which can be traced back to the optimization for the VMAT plan in the treatment planning system.

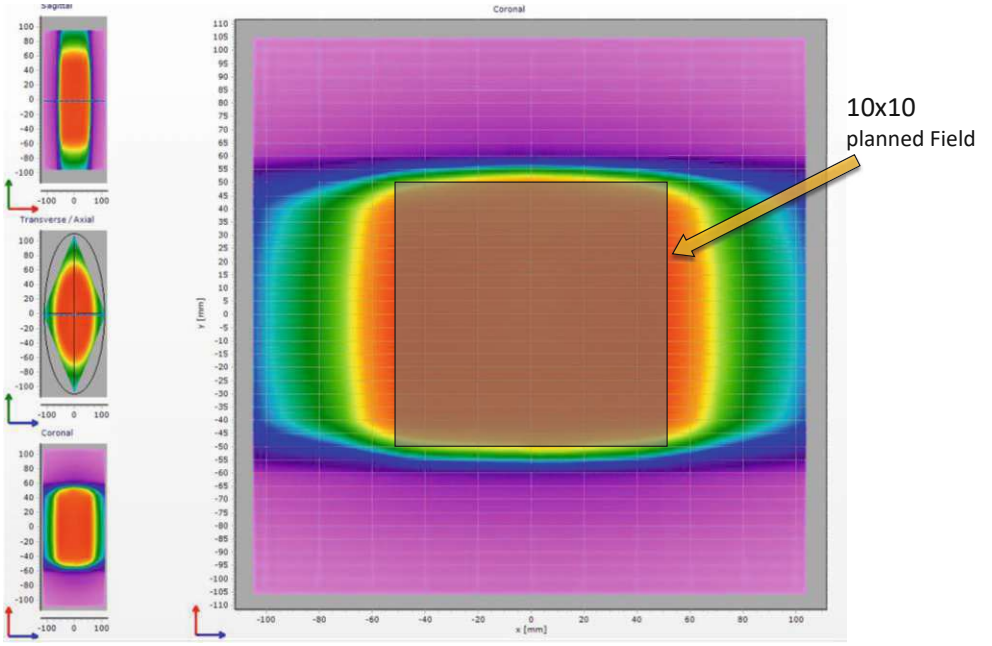

Figure 3.11: Axial view from the dose deviation of an open 10x10 cm^2 field

3.9 Delta 4 Phantom+

3.9.1 Overview and Specs

The Delta4 Phantom+ is a state-of-the-art 4D verification system designed for fast and accurate dose and treatment delivery verification. It is primarily used in pre-treatment quality assurance for advanced radiation therapy treatment plans. The Delta 4 phantom is capable of verifying the most common treatment therapy methods as IMRT and especially VMAT which is performed in this study. The system provides comprehensive QA for both patient and machine. It consists of two dual orthogonal detector planes which enable real measurements in the isocentric target region, enhancing the accuracy and efficiency of treatment plan verification. [3]

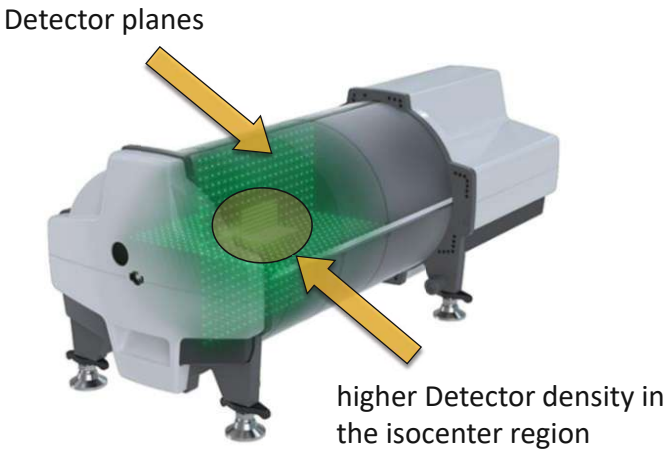

Figure 3.12: Scandidos Delta 4 Phantom+
[3]

Main Specifications

- **Phantom Material:** PMMA
- **Dimensions:** Diameter 22 cm, Length 40 cm, Total Length 71 cm
- **Detectors:**
  - Type: p-Si

  - Total number: 1069
  - Layout: Distributed on coronal and sagittal planes
  - Max field size: 20 x 38 cm^2 (when merging two consecutive measurements)

- **Wireless Communication:** Wi-Fi 802.11n

The Delta4 Phantom+ can measure several critical parameters in radiation therapy:

- **Dose Distribution:** Measures dose distribution in the isocentric region, providing instant pass/fail analysis by comparing delivered dose with planned dose.
- **Gantry Angle Verification:** Independent verification of beam delivery angles in real time using an inclinometer.
- **Machine QA:** Performs checks on beam constancy and Multi-Leaf Collimator performance.

The system's software performs a direct analysis and calculate parameters such as dose deviation, distance to agreement (DTA), gamma index, and dose-volume histograms.

3.9.2 Temperature dependency

The performance and accuracy of the Delta4 Phantom+ can be influenced by temperature variations in the storage room and the measurement environment. The phantom's detectors are made of p-type silicon (p-Si), which exhibits temperature-dependent behavior that can affect the measured dose distributions. It is crucial to account for these dependencies to ensure accurate and reliable measurements. A correction value can be applied to shift a potential over or under dose scale. Therefore it was necessary to do a reference measurement before every session to evaluate the temperature dependence correction value, to keep the whole data under the same conditions. [37]

4 Data

4.1 Data evaluation

The first step was the preparation of every treatment plan in the 'Raystation Treatmentplanning' program by (RaySearch Laboratories 2024, SWE). Therefore a copy of every plan had to be generated to reset the Gantry Space level at 2°, 3° and 4°. After that the optimization parameter could be set, so the RayStation algorithm optimize for 40 iterations, before calculating the final dose. This optimization process has been done for 40, 120, 240 and 360 iterations for most of the plans. The purpose of these repeating optimization process is to generate highly modulated plans, to see how the crucial parameters of the LINAC will behave. After all these iterations, written scripts (8) were applied to read out some of the parameters as mentioned before.

Treatment plans for the measurement

For the actual measurement on the LINAC to evaluate the Gamma Index, not all of the prepared treatment plant have been irradiated. For a better understanding, the measurement table of the irradiated plans and a table for the parameter analysis can be seen as following.

Category	Gantry Spacing (°)	Modulation (IT)	Patients	Total
Prostate	(2°, 3°, 4°)	120	5	15
Mamma	(2°, 3°, 4°)	120	5	15
HNO	(2°, 3°, 4°)	120	5	15
Total			15	45

Table 4.1: Total treatment plans prepared for measuring the Gamma Index depending on the gantry spacing

Also important to say is that the measurement for the gamma index of the gantry spacing related plans were performed under an iteration level of 120. The measurement for the modulated treatment plans are performed under a 4° gantry spacing level to have similar conditions.

Category	Gantry Spacing (°)	Modulation (IT)	Patients	Total
Prostate	4°	(40, 120, 240, 360)	2	8
Mamma	X	X	X	X
ENT	4°	(40, 120, 240, 360)	2	8
Total			4	16

Table 4.2: Total treatment Plans prepared for measuring the Gamma Index depending on the modulation

Treatment plans for the parameter analysis

The next table shows the number of treatment plans which are used for the evaluation and analysis of the crucial parameters such as MCS and will discussed in the following chapters.

Category	Gantry Spacing (°)	Modulation (IT)	Patients	Total
Prostate	(2°, 3°, 4°)	(40, 120, 240, 360)	5	60
Mamma	(2°, 3°, 4°)	(40, 120)	5	30
ENT	(2°, 3°, 4°)	(40, 120, "240")	5	56
Total			15	146

Table 4.3: Total treatment Plans for analyzing the critical parameters

4.2 Parameter description

Leaf Travel Value

The Leaf Travel Value quantifies the average motion of the multi-leaf collimator leaves during a treatment. This metric is particularly relevant for Volumetric Modulated Arc Therapy plans, where the MLC leaves continuously move to shape the radiation beam as the gantry rotates around the patient. The LTV provides a

measure of the efficiency of leaf movement during treatment, with higher values indicating more extensive leaf travel.

To compare a variation of treatment plans, such as different gantry spacing or different number of arcs, the LTV is normalized by the following formula:

$$\text{LTV} = \frac{2000\,\text{mm} - \text{LT Mean (mm)}}{2000\,\text{mm}} \tag{4.1}$$

LTMCS

The LTMCS value is just a combination of the two parameters (MCSv and LTV) which are described earlier. This index was introduced to integrate the impact of both leaf movement and the complexity of beam modulation, providing a more comprehensive measure of plan complexity.

The LTMCS is calculated by first normalizing the Leaf Travel (LT) as mentioned before using a predefined maximum value, creating a dimensionless index (LTi). This index is then multiplied by the MCSv, which ranges from 0 to 1, with lower values indicating higher modulation complexity. The resulting LTMCS value ranges then also from 0 to 1, where values closer to 1 indicate simpler plans with minimal leaf motion and modulation, and values closer to 0 indicate more complex plans with significant leaf travel and modulation similar to the existing MCSv. [29]

$$\text{LTMCS} = \text{LTV} \times \text{MCSv} \tag{4.2}$$

A/U

The A/U value is a metric used, specifically in the context of Volumetric Modulated Arc Therapy. This ratio is defined as the area of the aperture created by the multi-leaf collimator leaves divided by the circumference of the leaf aperture. The A/U value provides insight into the efficiency and complexity of the beam aperture shape during treatment delivery. [17]

A higher A/U value typically indicates a more efficient aperture shape, where the area is maximized relative to the perimeter, suggesting that the radiation is being

delivered more effectively over the target area. Conversely, a lower A/U value could suggest that the beam aperture is more irregular or elongated, potentially leading to less efficient delivery and higher modulation complexity.

Tongue and Groove

The Tongue-and-Groove (T&G) value is a metric used to describe the degree to which the side by side leaves of a multileaf collimator interlock in radiation therapy devices. The T&G design is an engineering feature where each leaf of the MLC has a protruding "tongue" on one side and a corresponding "groove" on the other side. When the leaves are closed, the tongue of one leaf fits into the groove of the opposite leaf, reducing the gaps between them and thus minimizing radiation leakage. The T&G value quantifies this interlocking feature, essentially representing how much the leaves overlap and interlock with one another. [7]

Monitor Units per centi Gray

The MU/cGy value is a critical parameter which can be used to quantifie the efficiency of radiation delivery. It represents the number of monitor units required to deliver one centigray (cGy) of radiation dose to a specified point, typically within the target volume. A lower MU/cGy value indicates a more efficient delivery, where fewer monitor units are needed to achieve the desired dose. This value is important for evaluating the overall efficiency and it helps in minimizing treatment time and reducing radiation exposure to healthy tissues.

5 Results

5.1 Analysis of the Parameters

First of all, the MCS values of all 146 treatment plans were analyzed to determine the correlation with the number of iterations and the gantry spacing level. This analysis aims to investigate the relationship between plan complexity and various LINAC parameters. One of the primary objectives of this study is to understand how plan complexity is influenced by different configurations of the LINAC.

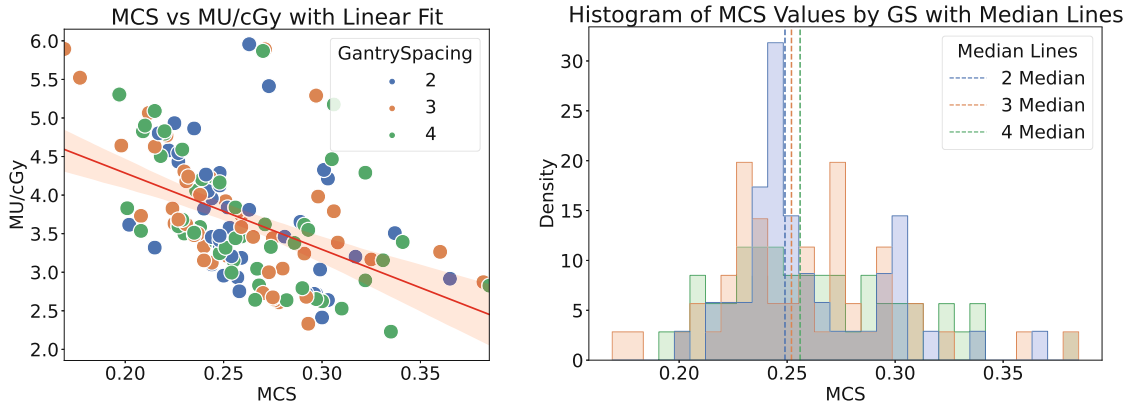

Figure 5.1: Linear regression through all data points and distribution plot of the MCS regarding to the gantry spacing level.

Since the MCS value is indirect proportional to the complexity of a plan, the plot 5.1 clearly indicates that higher plan complexity gets an increased number of monitor units for irradiation but do not change tremendously with other gantry spacing levels. To provide a clearer perspective, a linear regression was performed on all data points. Despite this, the average MCS with respect to gantry spacing across the three different cases does not exhibit significant variation, as observed in the distribution plot. However, when considering the number of iterations taken

by the optimization algorithm in the treatment planning system, a distinct trend emerges: treatment plans become more complex with increasing optimization steps. Conversely, the leaf travel distance remains relatively constant.

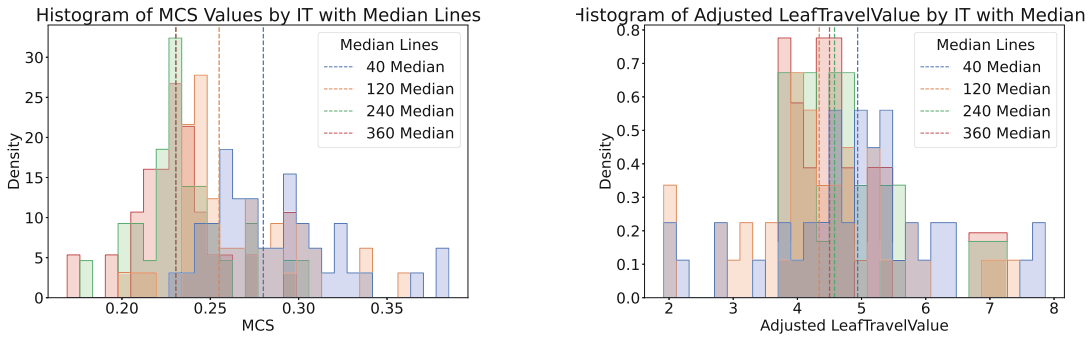

Figure 5.2: Distribution plots of the MCS and the Leaf Travel regarding the number of iterations during the optimization process

The next parameter which has been observed was the leaf travel. For a better comparison of the average leaf travel per level gantry spacing, a normalization of the values for each level has to be done. The reason therefore is, that at 2 level gantry spacing the LINAC has automatically more checkpoints to go through, but the leafs need to move less per checkpoint, too. To provide a acceptable validation of this parameter, it is important to implement a normalization for the 2°, 3° and 4° level. According to this setup we can clearly see the the difference between the raising optimization parameter and the gantry spacing. The median of the density for the gantry spacing is nearly independent and has no major difference compare to the optimization parameter.

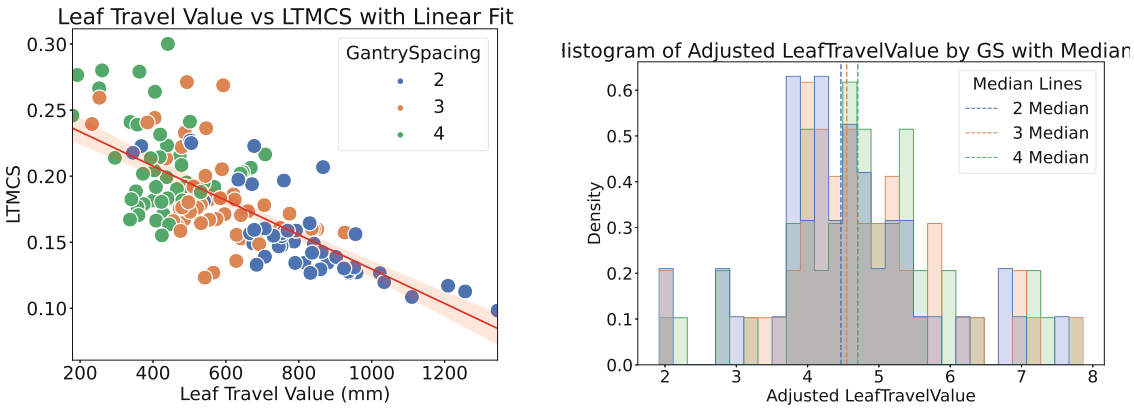

Figure 5.3: Linear regression through all data points and distribution plot of the Leaf Travel regarding to the gantry spacing level

After the examination of the correlations and trends, we can turn our attention to plotting all the crucial parameters for each case. This will help, gain a clearer understanding of how these parameters behave under same conditions.

Having examined the correlations and trends, th crucial parameters for each case are visualized, focusing on different gantry spacing levels. The following boxplots illustrate the distributions of key metrics such as MCS (Modulation Complexity Score), Leaf Travel Value, A/U, TaG, MUCGy, and LTMCS for gantry spacings of 2, 3, and 4 degrees across different cases (Prost, Mamma, and ENT).

- The boxplot for the MCS (Modulation Complexity Score) demonstrates how the complexity of the treatment plans varies with changes in gantry spacing. This visualization highlights the results from before.
- The boxplot for the Leaf Travel Value shows how the movement of the multileaf collimator leaves varies across different gantry spacings. This metric is crucial for understanding the mechanical workload on the LINAC.
- The boxplots for A/U, TaG, Mu/cGy, and LTMCS each provide insights into the distribution of these parameters with respect to gantry spacing.

Secondly the number of the iteration steps has been taken into account and evaluated for the different parameters mentioned before. There every path for each group either prostate, ENT or mamma can be observed very clearly. Outstanding, mamma treatment plans has been stopped calculating by the treatment planning

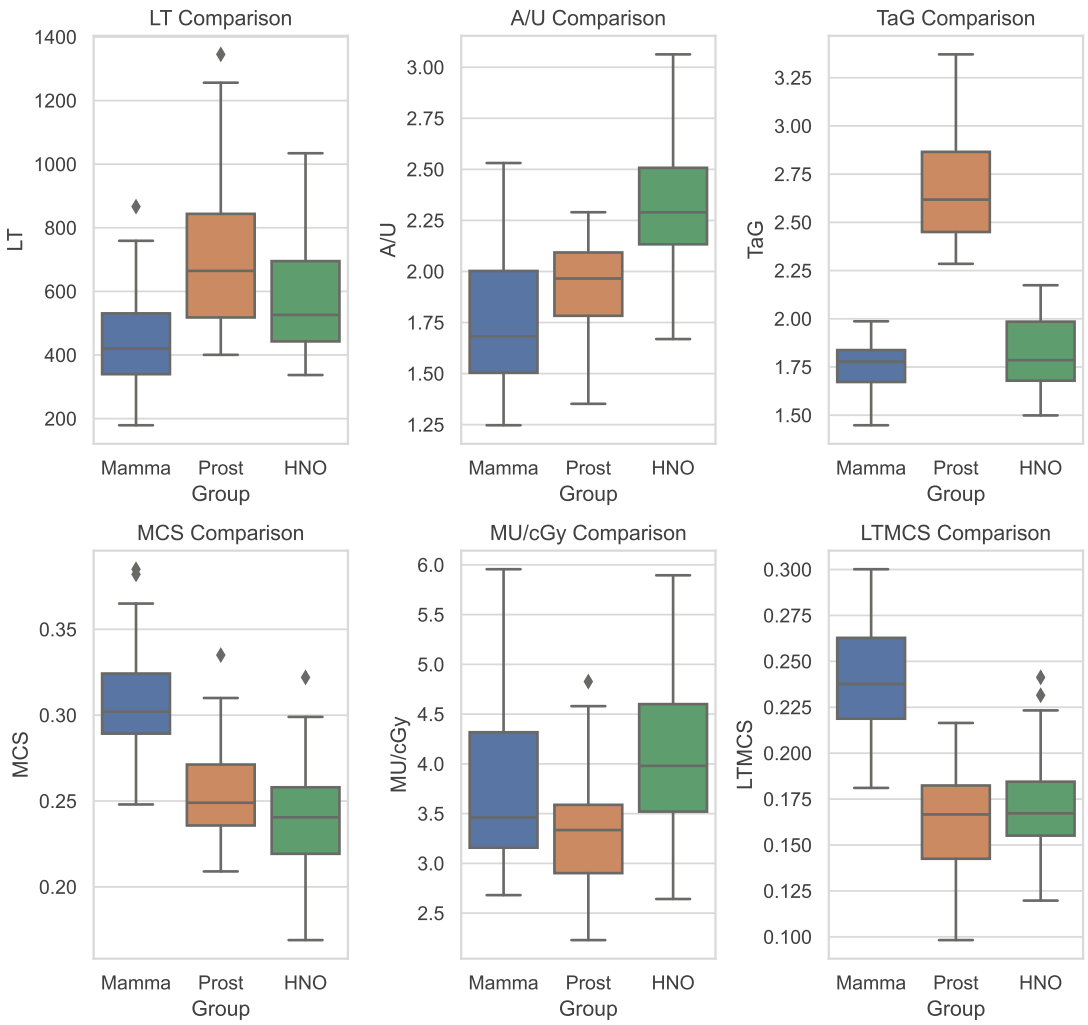

Figure 5.4: Boxplots for every evaluated parameter for each category

system, because the best solution according to the optimizing algorithm has been already found after 120 iterations steps. That is why these two boxplots are missing.

Additionally, a pairplot for further analyzation of all the relationships between these parameters by gantry spacing has been included. This pairplot offers a multi-dimensional perspective, allowing us to observe potential correlations between different parameters simultaneously. For example, the pairplot reveals how the MCS values correlate with the number of iterations, Leaf Travel Value, MU/cGy, TaG, and LTMCS across different gantry spacings, as mentioned in the sections before.

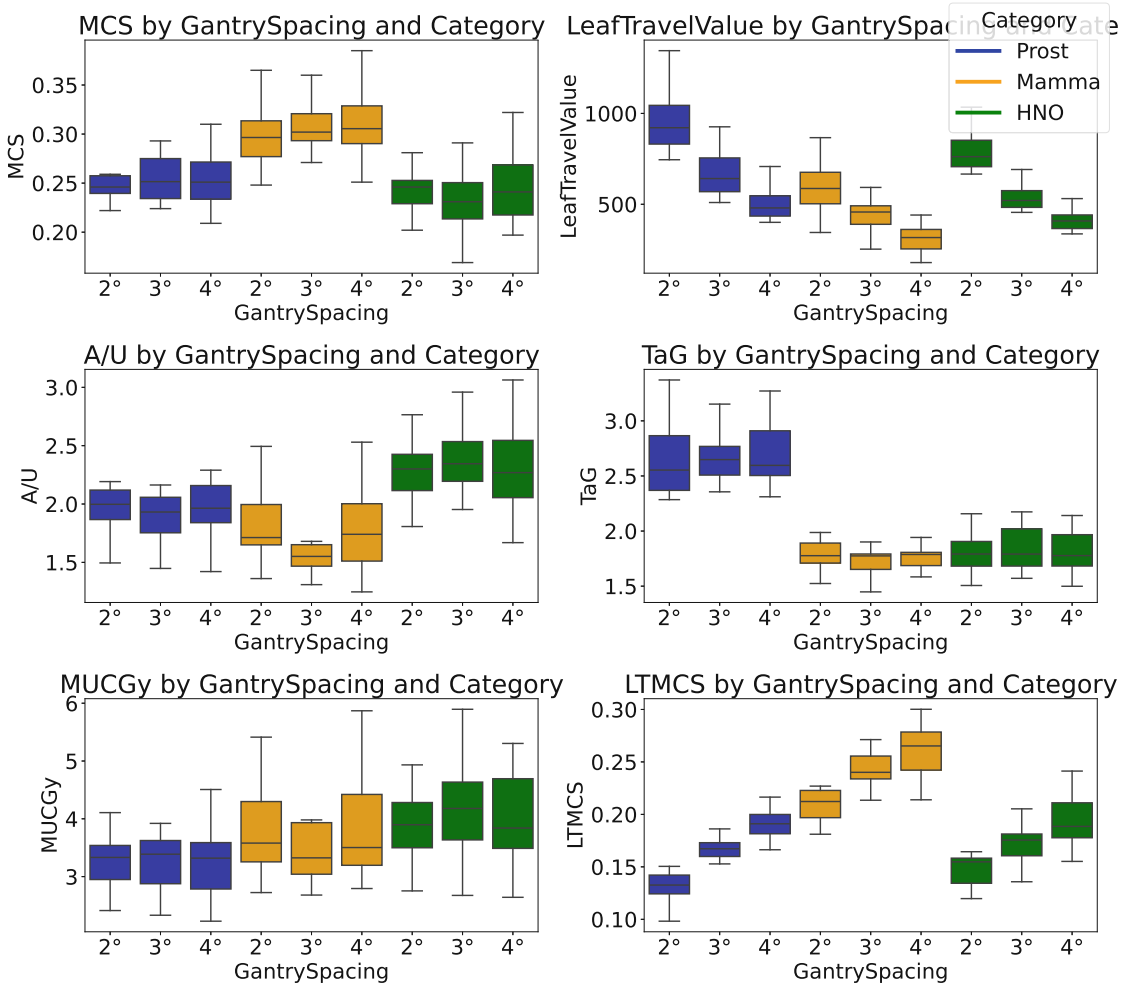

Figure 5.5: Boxplots for every evaluated parameter selected by the gantry spacing for each category

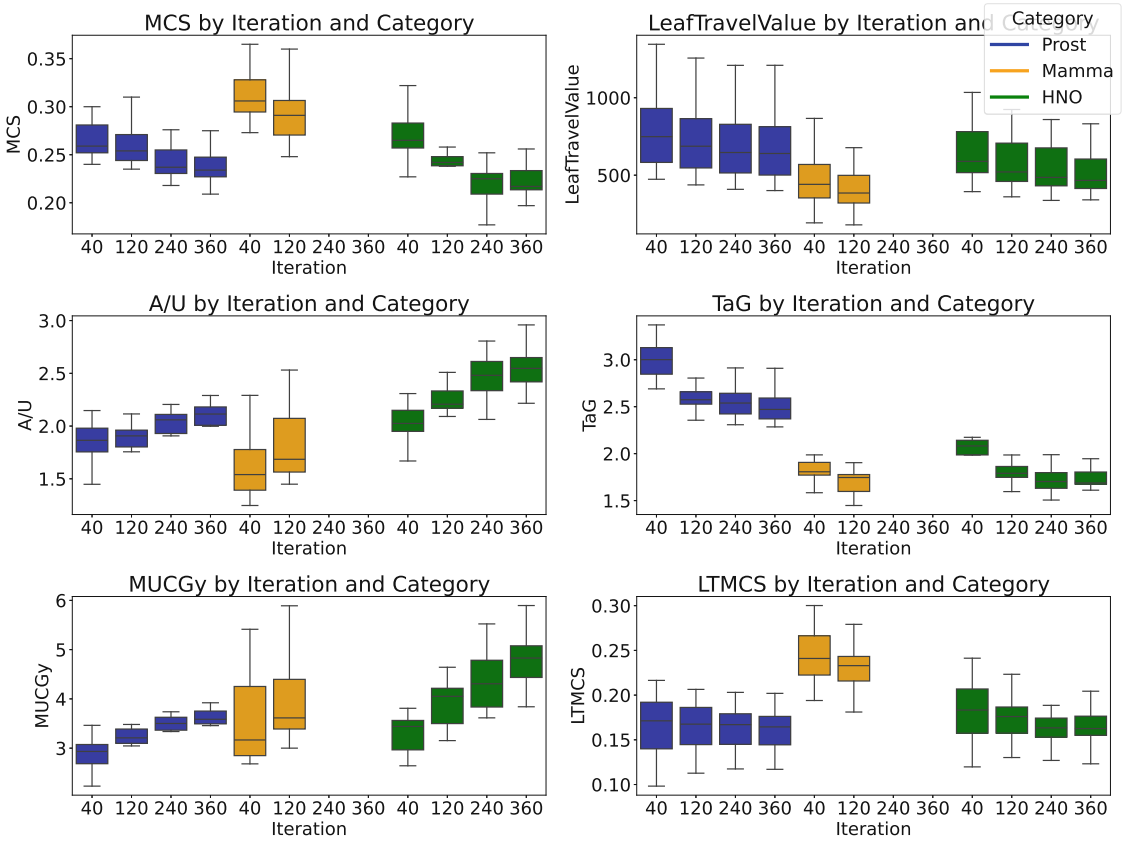

Figure 5.6: Boxplots for every evaluated parameter selected by the number of iterations for each category

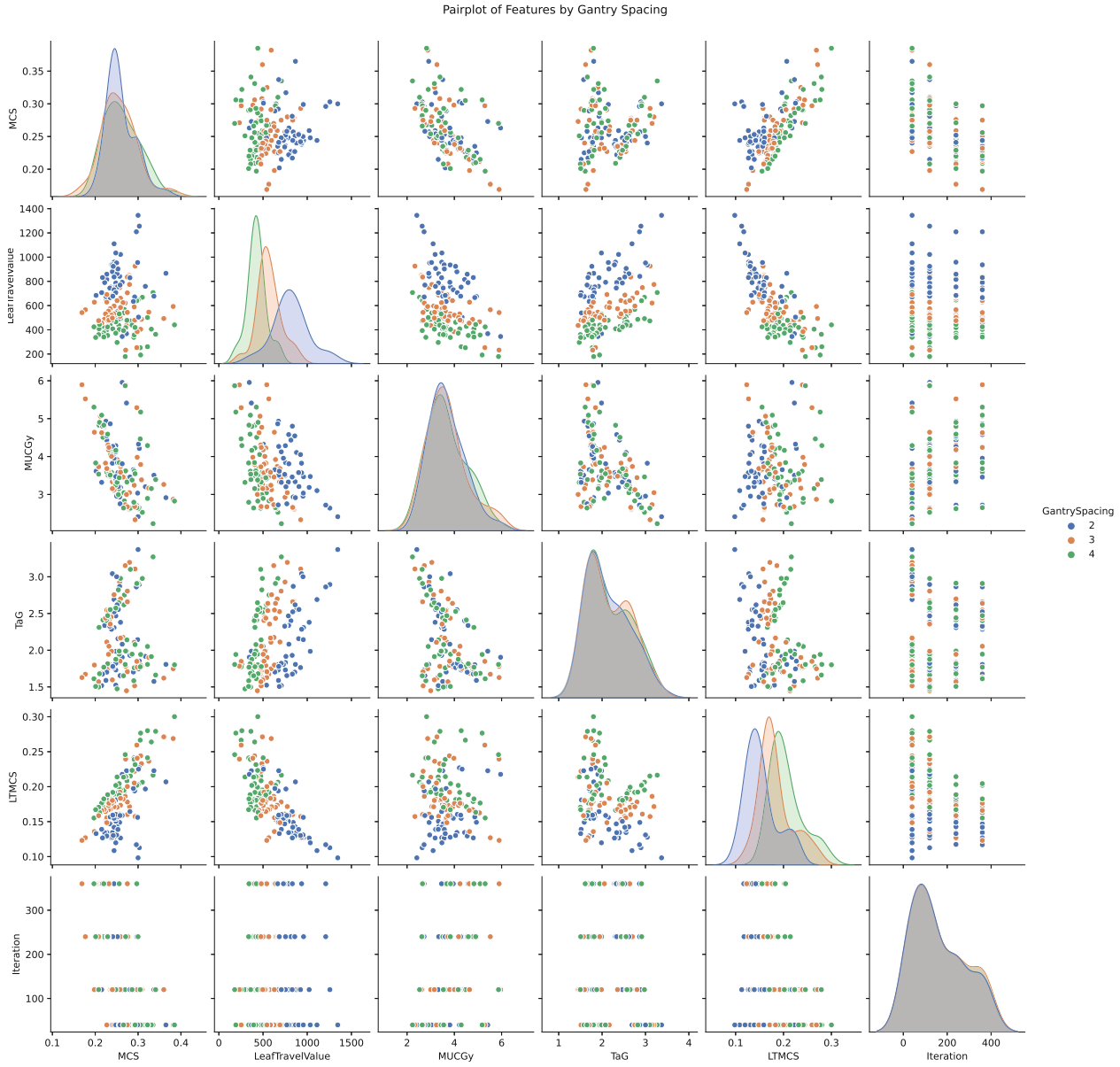

Figure 5.7: This pairplot illustrates the relationships between key parameters such as MCS, Leaf Travel Value, MUCGy, TaG, LTMCS, and the number of iterations, across different gantry spacings (2, 3, and 4 degrees)

5.2 Gamma passing rates of different Gantry spacing levels

The following figures are the results of the QA measurements of the Delta4+ Phantom. The gamma index has been measured and evaluated for 3%/3mm and 2%/2mm. Presenting the results from the measurement table [4.1] are now set against the evaluated critical parameters of the LINAC gathered and analyzed in the chapter before.

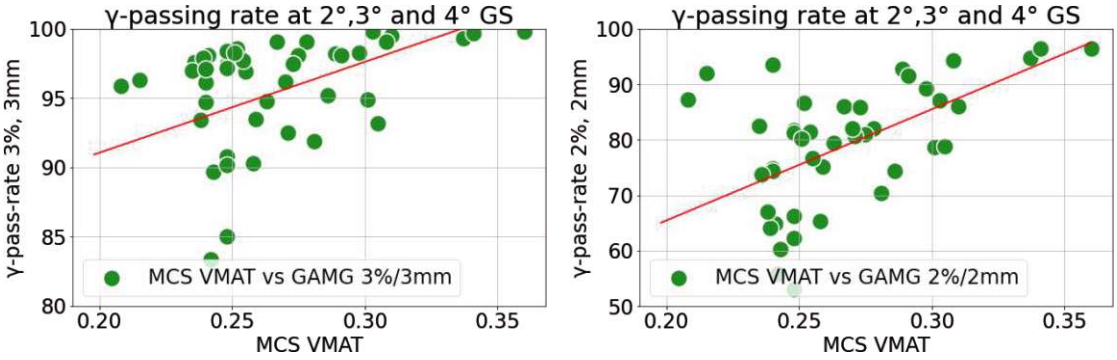

Figure 5.8: Gamma passing rates compared to the complexity score

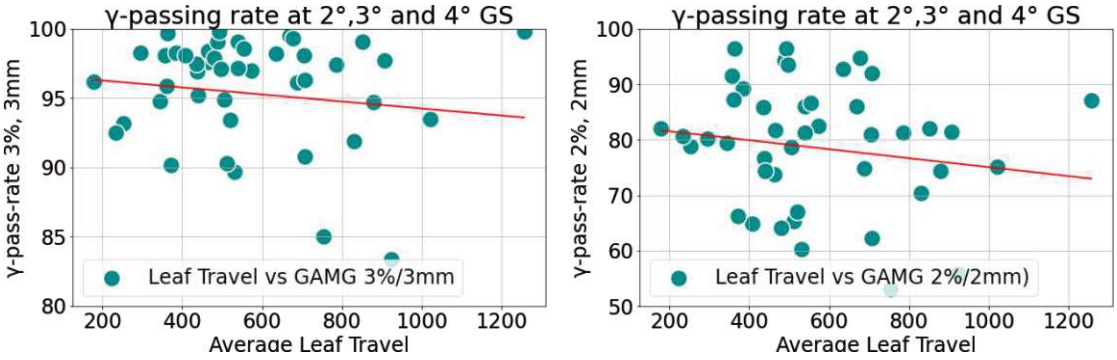

Figure 5.9: Gamma passing rates compared to the average leaf travel

45 plans has been measured for the evaluation regarding to the gantry spacing and 16 plans regarding to the modulation, and the overall statistics about the gamma passing rates are presented in the table [5.1] below.

As it can clearly be seen that most of the plans regardless of the gantry spacing or number of iterations has a pretty high pass rate. In general there is a lowest pass rate validation barrier which confirms treatment plans for a clinical application.

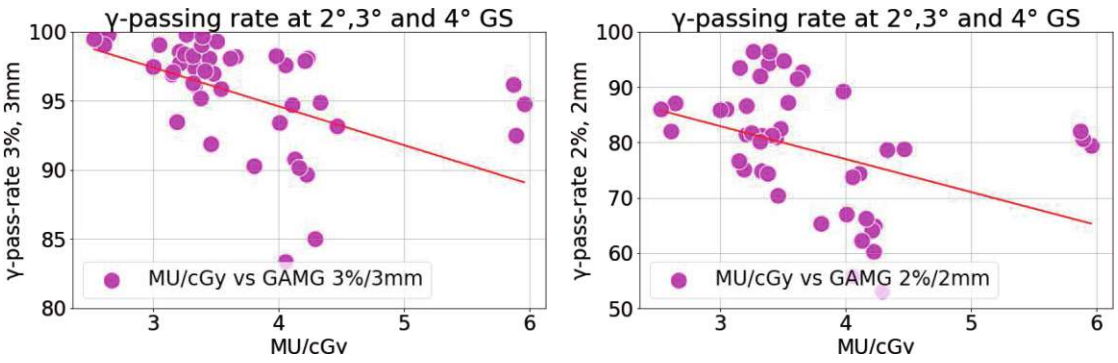

Figure 5.10: Gamma passing rates compared to the number of MU/cGy

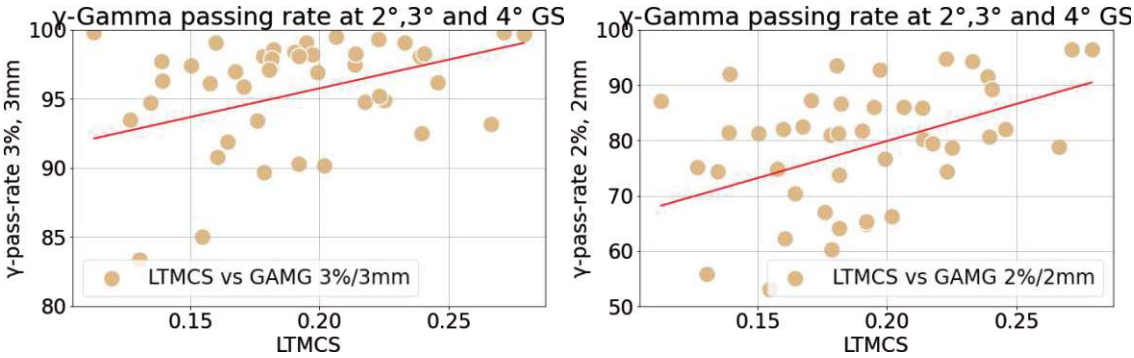

Figure 5.11: Gamma passing rates compared to combined LTMCS

This value can differ from hospital to hospital but it is mostly set to 90 % and therefore most of the plans would have been passed this criterion anyway.

Statistic	3%/3mm	2%/2mm
Mean pass-rate(%)	95.34	78.54
Max pass-rate(%)	99.80	96.50
Min pass-rate(%)	74.60	44.70
Percentage of plans > 95%	66.67%	4.44%
Percentage of plans > 90%	91.11%	17.78%

Table 5.1: Summary statistics for γ-pass-rates (3%/3mm and 2%/2mm)

5.2.1 Correlation analysis

To get a more meaningful view about the correlation between the plan parameters and the observed passing rates, a common Pearson correlation analysis was made and checked plus confirmed for statistical significance for every Pearsons value ($p < 0.05$). Generally the Pearson correlation analysis is a statistical method used to measure the strength and direction of the linear relationship between two continuous variables. The result, called the Pearson correlation coefficient (r), ranges from -1 to 1. A value of 1 indicates a perfect positive correlation, -1 indicates a perfect negative correlation, where 0 indicates no linear correlation. [11] As we can see at the results of the test, they confirm the seen correlation between the crusial parametes like MCS and leaf travel with the gamma passing rate as seen in the Figures [5.8][5.9][5.10][5.11].

Variable	3%/3mm	2%/2mm
Leaf_travel	-0.114728	-0.148591
MCSv	0.454174	0.563520
LTMCS	0.341236	0.446050
MU/cGy	-0.440578	-0.379274

Table 5.2: Pearson Correlation Coefficients for Variables with γ-pass-rate

Splitting up the evaluated data into their gantry spacing category leads to more visible results in terms of the significance of it. As we wanted to prove an impact from the gantry spacing to the performance of the different treatment plans, there is indeed a clear difference as seen in the boxplot [5.12].

For a better overview and a more general comparison of the gamma value depending on the gantry spacing value, a boxplot for each group can be seen below.

Parameter	2°GS	3°GS	4°GS
MCSv	0.265	0.264	0.266
LTMCS	0.163	0.193	0.212
Leaf travel	4.248	4.496	4.503
MU/cGy	3.771	3.694	3.746
γ-pass-rate 3%/3mm	94.3	94.7	96.9
γ-pass-rate 2%/2mm	77.3	78.9	79.3

Table 5.3: Mean values for each parameter by GS category (2°GS, 3°GS, 4°GS).

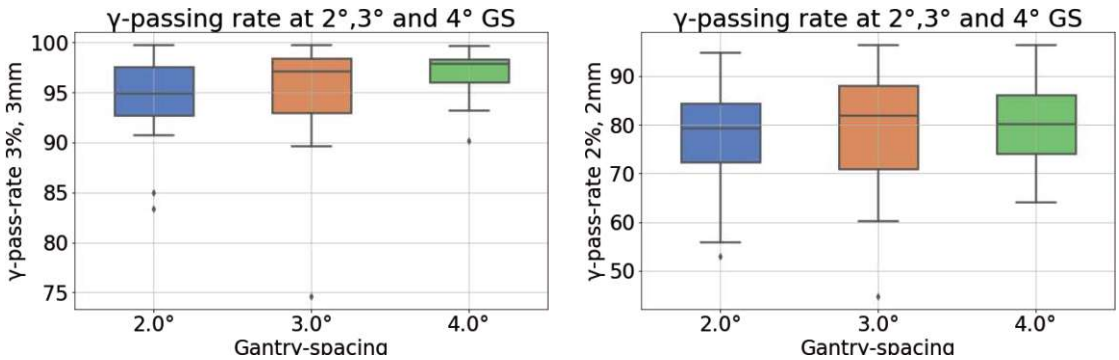

Figure 5.12: Boxplots of the gamma passing rates for each group of the gantry spacing

5.3 Gamma passing rates of different various modulated plans

The second part of the Delta 4 measurement contained the different number of iteration in the treatment planning process. As mentioned in the chapters before, a highly modulated plan has different crucial parameters like leaf travel or MCS than a common plan. The usual optimization steps in clinical usage for a patient application is around 80 to 120 to get the best balance of modulation and dose accuracy but its of course always depending on the various properties of the patients geometry.
As we can gather from the measurement table [4.2], 4 treatment plans (2 ENT and 2 Prostate) were taken and highly modulated up to 360 iteration steps. The evaluation of the gamma passing rate should give insights how these modulated plans behave and if there is a some evidence for an optimum of modulation.

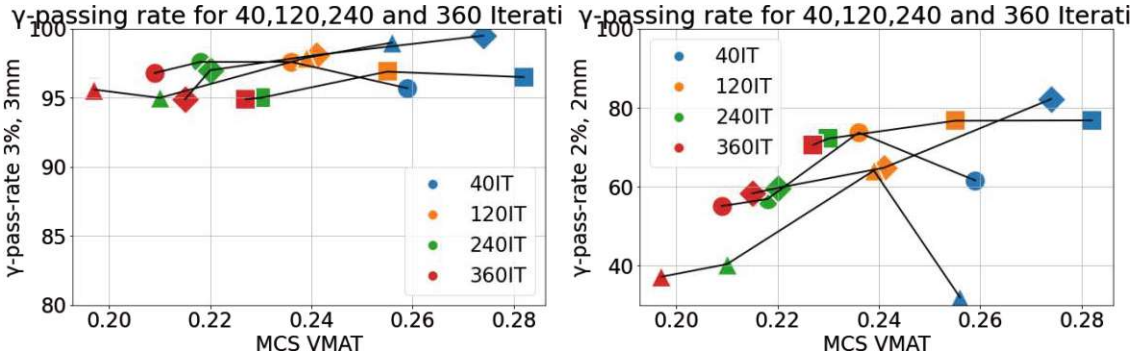

Figure 5.13: Gamma passing rates compared to the MCSv depending on the number of IT

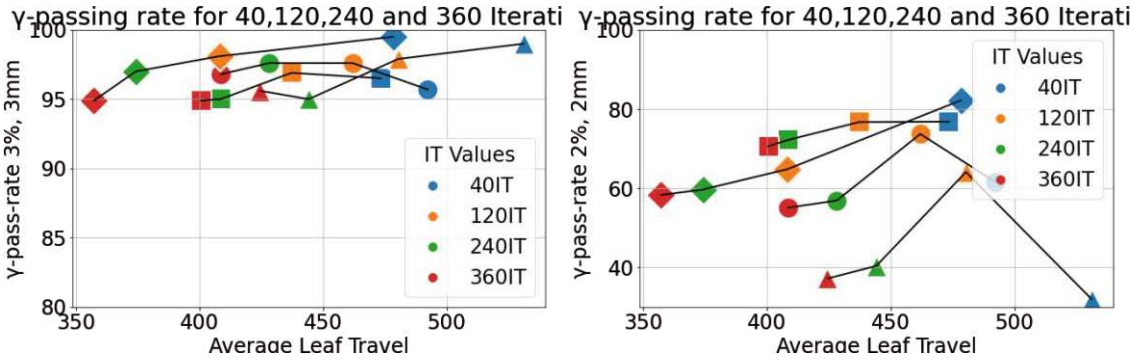

Figure 5.14: Gamma passing rates compared to the Leaf travel depending on the number of IT

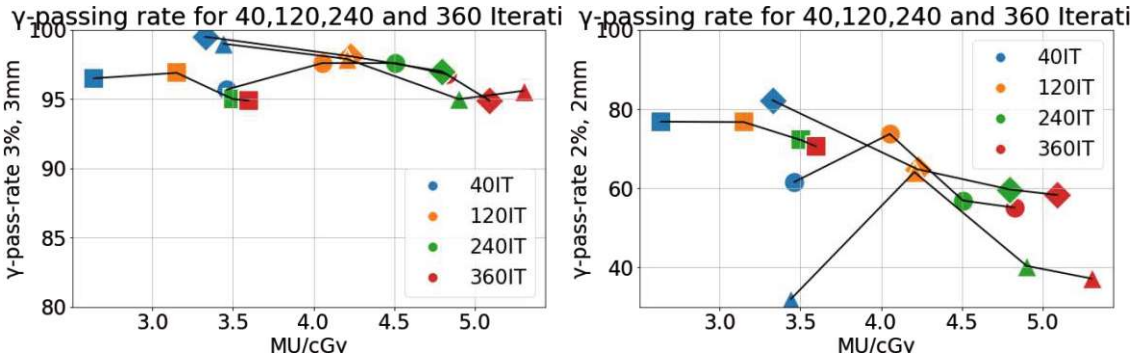

Figure 5.15: Gamma passing rates compared to the MU/cGy depending on the number of IT

Every mean values for the common parameters has gathered in the table below for a better overview and separation of the different modulation steps. Slight changes in the passing rates can be observed at the different criterions but that will be discussed

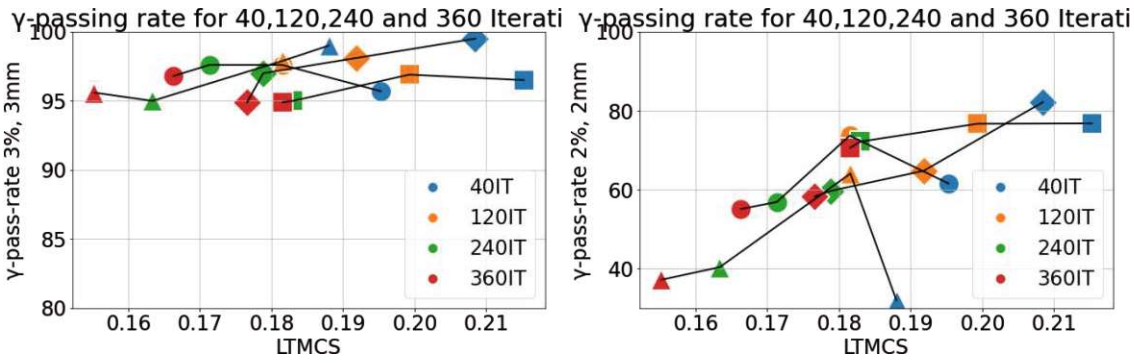

Figure 5.16: Gamma passing rates compared to the LTMCS depending on the number of IT

in the following chapters.

Metric	40IT	120IT	240IT	360IT
MCSv	0.27	0.24	0.22	0.21
LTMCS	0.20	0.19	0.17	0.17
Leaf Travel	493.84	446.95	413.78	397.74
MU/cGy	3.22	3.91	4.43	4.70
γ-pass-rate 3%/3mm	97.67	97.62	96.15	95.55
γ-pass-rate 2%/2mm	63.15	69.82	57.30	55.30

Table 5.4: Mean values for different iteration groups.

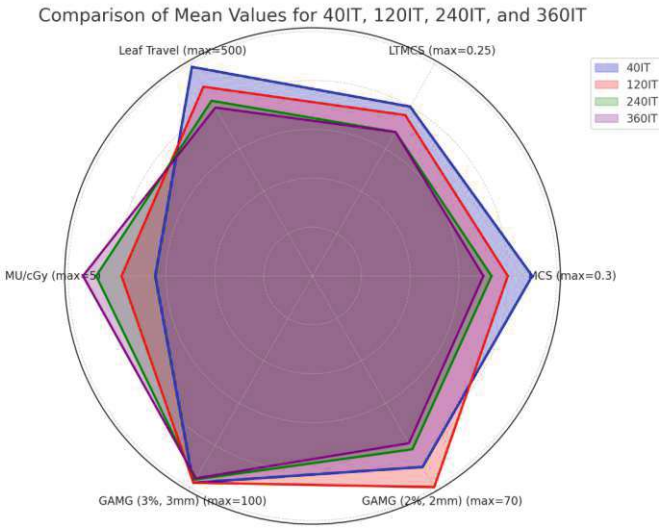

Figure 5.17: Radar chart comparing the mean values of key parameters across four modulation intensities (40IT, 120IT, 240IT, and 360IT).

6 Discussion

Gantry Spacing

Results of 45 near realistic patient treatment plans were analyzed regarding to the gamma passing rate to observe any relationships between the gantry spacing or the modulation iteration steps and the critical parameters of the LINAC.
The main assumption has clearly been proven. The more complex a treatment plan will get, the gamma passing rate, either with the 3%/3mm or 2%/2mm criterion, is dropping significantly. Fig. [5.8] shows a direct proportionality of the MCS value and the gamma passing rate for all given treatment plans. This connection can also be seen at the other critical parameters such as the average leave travel or the MU/cGy value which both leads to the result that the smaller both values get, the better will be the gamma passing rate. Fig. [5.9]&[5.10] The Pearson correlation test therefore confirms the strongly related parameters. These results has also been proven by "Laura Masi" in the paper [29] where also critical parameters has been observed regarding to the gamma passing rate.
Secondly the results of this study highlight a recognizable impact of gantry spacing on the Gamma Index, a key metric used to evaluate the accuracy of radiation dose delivery in VMAT treatments. As gantry spacing decreases, from 4° to 2°, the variance of the gamma passing rates decreased which can be seen in Fig. [5.12]. This trend suggests maybe that smaller steps in gantry spacing tendentially leads to worse gamma passing rated independently from the complexity of a plan. Fig. [5.1]
For better statistical understanding of these results a t-test is conducted to determine if there are statistically significant differences between the means of the gamma passing rate by each gantry spacing group.

Since the p-values in the results of the test are all above the common significance threshold of 0.05, significant differences in the Gamma Index values for different

GS1	GS2	Test	t-statistic	p-value
2.0°	3.0°	3%/3mm	-0.201881	0.841581
2.0°	3.0°	2%/2mm	-0.332206	0.742244
2.0°	4.0°	3%/3mm	-1.858027	0.077112
2.0°	4.0°	2%/2mm	-0.488778	0.629082
3.0°	4.0°	3%/3mm	-1.234378	0.232693
3.0°	4.0°	2%/2mm	-0.082383	0.935012

Table 6.1: T-test results for Gamma Index comparison at different gantry spacings

gantry spacings suggests that the changes in gantry spacing (from 2.0° to 4.0°) do not substantially impact the dosimetric accuracy, as measured by the Gamma Index. This indicates that within the studied range, varying the gantry spacing does not lead to meaningful differences in treatment quality.

Modulation

The four different plans has been observed to find a common behavior of a gaining modulation. For a better comparison, every plan was measured with the same gantry spacing level of 4°. And indeed, as we can see in the Fig. [5.17] with the 3%/3mm gamma criterion, every path is getting more complex for higher modulation. The correlation between the modulation and the complexity has also been proven in the chapter of the analysis of the parameters [5.1]. At Fig. [5.2] it can clearly be seen that the median of all evaluated plans goes more complex with gaining iteration steps. The same pattern can also be observed for the average leaf travel and the MU which are also raising or falling with higher iteration steps. And that is exactly what we initially expected. The planning system algorithm searches for the best solution with more and more steps which automatically leads to slightly more changes in the parameters. And this can be an indicator for a more complex shape of the MLC that affect the A/U ratio becoming a more complex treatment plan for the LINAC. The LINAC itselfs tries to compensates that with changes in the MU/cGy trying to still fulfill the starting boundery conditions.
If we have a look at the stricter criterion with 2%/2mm gamma passing rate, the behaviour with gaining optimization steps is not so straight foreword as before. The triangular and circle shaped data points in the figures [5.13],[5.14],[5.15] and [5.16] have a clear maximum at 120 iteration steps. That might indicate an optimum

of modulation where complexity, leaf travel and the other parameters are so well balanced that they lead to the best outcome of a treatment plan. But this pattern can only be observed for this sharper gamma passing rate and only for these two plan paths.

7 Conclusion

This study successfully evaluated critical parameters influencing the complexity and deliverability of Volumetric Modulated Arc Therapy treatment plans, specifically focusing on gantry spacing, modulation complexity, and critical metrics. The use of the Modulation Complexity Score and gamma index provided valuable insights into the relationship between plan complexity and dosimetric accuracy.

The results demonstrated that higher plan complexity, as indicated by lower MCS values, generally correlates with increased monitor units required for irradiation and challenges in maintaining dose accuracy. The gantry spacing played a visible role in plan complexity, with smaller spacings allowing for a bit precise control over dose distribution but at the cost of increased planning and delivery complexity. However, despite these variations, the study found that leaf travel distances remained relatively consistent across different levels of optimization, suggesting that leaf motion efficiency is maintained regardless of plan complexity.

Regarding to the outcome of this study there were some points that should be considered for future work that can be done in this field of theoretical radiation therapy. Especially in therms of modulation. As we could observe with various gamma passing rate criterions, different patterns of the modulation paths could be seen, so there maybe exist an optimum of iterations steps which is perfectly equilibrate in terms of complexity accuracy and treatment duration.

8 Appendix

8.1 Read Leaf Travel script

```
from connect import *
from math import fabs

patient = get_current("Patient")
case = get_current("Case")
plan = get_current("Plan")
beamset = get_current("BeamSet")

leaf_travels = [0.] * 80
leaf_openings = [False] * 80


for beam in beamset.Beams:
    for Seg in beam.Segments:
        start = int(40 - 2 * fabs(Seg.JawPositions[2]))
        ende = int(start + 2 * fabs(Seg.JawPositions[2]) + 2 * fabs
    (Seg.JawPositions[3]) - 1)
        previous_positions = Seg.LeafPositions[0][:]
        for i in range(start, ende + 1):
            diff = Seg.LeafPositions[1][i] - Seg.LeafPositions[0][i
    ]
            if diff > 0:
                leaf_travels[i] += fabs(Seg.LeafPositions[1][i] -
    previous_positions[i])
                leaf_openings[i] = True
            previous_positions[i] = Seg.LeafPositions[1][i]

total_travel = sum(leaf_travels[i] for i in range(80) if
    leaf_openings[i])
```

```
active_leaves = sum(1 for i in range(80) if leaf_openings[i])
average_travel = total_travel / active_leaves if active_leaves > 0
    else 0

output_data = f"Average Leaf Travel (for active leaves): {
    average_travel:.2f} mm\n"

output_file_path = "M:\\Master_Auswertung\\HNO\\HNO_5\\2_GS\\240_IT
    \\LT_HNO5_2GS_240IT.txt"
with open(output_file_path, 'w') as file:
    file.write(output_data)
    file.close()
```

Listing 8.1: Python example

8.2 Read DVH values script

```
from connect import get_current

def write_dose_statistics(filename, results):
    with open(filename, 'w') as file:
        file.write('ROI, D95 (Gy), D50 (Gy)\n')
        for roi, stats in results.items():
            file.write(f"{roi}, {stats['D95']:.2f}, {stats['D50
    ']:.2f}\n")

        file.close()

from connect import *

def main():
    patient = get_current("Patient")
    case = get_current("Case")
    plan = get_current("Plan")
    dose = plan.TreatmentCourse.TotalDose

    results = {}

    for roi in case.PatientModel.RegionsOfInterest:

```

```
            dose_values = dose.GetDoseAtRelativeVolumes(RoiName=roi
    .Name, RelativeVolumes=[0.95, 0.50])
            results[roi.Name] = {
                'D95': dose_values[0],
            }

    filename = "M:\\Master_Auswertung\\HNO\\HNO_5\\2_GS\\240_IT\\
    DVH_HNO5_2GS_240IT.txt"
    write_dose_statistics(filename, results)
    print(f"Dose statistics written to {filename}")

if __name__ == "__main__":
    main()
```

Listing 8.2: Python example

8.3 Read Linac parameters script

```

from connect import *
from numpy import mean, multiply, array, logical_or, invert, append

def write_to_file(filename, data):

    with open(filename, 'w') as file:
        file.write(data)
        file.close()

def getQAParameters():
    plan = get_current("Plan")
    beamset = get_current("BeamSet")

    plan_name = plan.Name

    MCS = []
    MU_beams = []

    a = 0.5
    counter = 0
    beam_mu = 0
```

```
    F_beam = []
    TG_beam = []
    loops = []

    for beam in beamset.Beams:
        Li_AAV = []
        Li_LSV = []
        Li_MU = []

        Leafs = []

        beam_mu += beam.BeamMU
        MU_beam = beam.BeamMU

        F = 0
        TaG = 0
        segcounter = 0.
        closed_loops = 0.

        Leafs = [0] * 80

        zz = -1
        start = [0] * len(beam.Segments)
        ende = [0] * len(beam.Segments)
        start2 = [0] * len(beam.Segments)
        ende2 = [0] * len(beam.Segments)

        for Seg in beam.Segments:
            zz += 1
            start[zz] = int(40 - 2 * abs(Seg.JawPositions[2]))
            ende[zz] = int(start[zz] + 2 * abs(Seg.JawPositions[2])
 + 2 * abs(Seg.JawPositions[3]) - 1)
            start2[zz] = int(40 + 2 * Seg.JawPositions[2])
            ende2[zz] = int(40 + 2 * Seg.JawPositions[3])
            for i in range(start[zz], ende[zz] + 1):
                diff = Seg.LeafPositions[1][i] - Seg.LeafPositions
[0][i]
                if diff > Leafs[i]:
                    Leafs[i] = diff

```

```
61          aav_norm = sum(Leafs)
62
63          zz = -1
64
65          for Seg in beam.Segments:
66              zz += 1
67              closed_loops += 1.
68              segcounter += 1.
69              MU = Seg.RelativeWeight * MU_beam
70
71              TG = 0
72              A = 0
73
74              A = sum((Seg.LeafPositions[1][range(start2[zz], ende2[
    zz])] - Seg.LeafPositions[0][range(start2[zz], ende2[zz])]) * a)
75
76              U = Seg.LeafPositions[1][start2[zz]] - Seg.
    LeafPositions[0][start2[zz]] + \
77                  Seg.LeafPositions[1][ende2[zz] - 1] - Seg.
    LeafPositions[0][ende2[zz] - 1] + \
78                  2 * (ende2[zz] - start2[zz]) * a
79
80              idx = array(range(start2[zz], ende2[zz] - 1))
81
82              bool1 = logical_or(Seg.LeafPositions[0][idx] > Seg.
    LeafPositions[1][idx + 1],
83                                 Seg.LeafPositions[0][idx + 1] > Seg.
    LeafPositions[1][idx])
84              closed_loops += sum(bool1)
85              U += sum(bool1 * (Seg.LeafPositions[1][idx] - Seg.
    LeafPositions[0][idx]))
86              U += sum(invert(bool1) * abs(Seg.LeafPositions[0][idx]
    - Seg.LeafPositions[0][idx + 1]))
87              TG += sum(invert(bool1) * abs(Seg.LeafPositions[0][idx]
     - Seg.LeafPositions[0][idx + 1]))
88
89              bool2 = logical_or(Seg.LeafPositions[1][idx] < Seg.
    LeafPositions[0][idx + 1],
90                                 Seg.LeafPositions[1][idx + 1] < Seg.
    LeafPositions[0][idx])
```

```
            U += sum(bool2 * (Seg.LeafPositions[1][idx + 1] - Seg.
LeafPositions[0][idx + 1]))
            U += sum(invert(bool2) * abs(Seg.LeafPositions[1][idx]
- Seg.LeafPositions[1][idx + 1]))
            TG += sum(invert(bool2) * abs(Seg.LeafPositions[1][idx]
 - Seg.LeafPositions[1][idx + 1]))

            F += MU * U / A
            H = (ende2[zz] - start2[zz]) * a
            TaG += MU * TG / H

            diff = 0.

            p_max_left = -1000.
            p_min_left = 1000.
            p_max_right = -1000.
            p_min_right = 1000.

            aav_sum = 0.

            idx = array(range(start[zz], ende[zz] + 1))
            p_max_left = max(append(Seg.LeafPositions[0][idx],
-1000))
            p_min_left = min(append(Seg.LeafPositions[0][idx],
1000))
            p_max_right = max(append(Seg.LeafPositions[1][idx],
-1000))
            p_min_right = min(append(Seg.LeafPositions[1][idx],
1000))

            aav_sum += sum(Seg.LeafPositions[1][idx] - Seg.
LeafPositions[0][idx])

            pos_max_left = p_max_left - p_min_left
            pos_max_right = p_max_right - p_min_right

            N = 2 * abs(Seg.JawPositions[2]) + 2 * abs(Seg.
JawPositions[3])

            idx = array(range(start[zz], ende[zz]))
```

```
122
123             lsv_sum_left = pos_max_left * len(idx) - sum(abs(Seg.
    LeafPositions[0][idx] - Seg.LeafPositions[0][idx + 1]))
124             lsv_sum_right = pos_max_right * len(idx) - sum(abs(Seg.
    LeafPositions[1][idx] - Seg.LeafPositions[1][idx + 1]))
125
126             if pos_max_left == 0. and pos_max_right != 0.:
127                 LSV_S = lsv_sum_right / ((N - 1) * pos_max_right)
128             elif pos_max_left != 0. and pos_max_right == 0.:
129                 LSV_S = lsv_sum_left / ((N - 1) * pos_max_left)
130             elif pos_max_left == 0. and pos_max_right == 0.:
131                 LSV_S = 1.
132             else:
133                 LSV_S = (lsv_sum_left * lsv_sum_right) / ((N - 1) *
     pos_max_left * (N - 1) * pos_max_right)
134
135             AAV_S = aav_sum / aav_norm
136             MU_S = Seg.RelativeWeight
137             Li_AAV.append(AAV_S)
138             Li_LSV.append(LSV_S)
139             Li_MU.append(MU_S)
140
141         A = len(Li_AAV)
142
143         loops.append(closed_loops / segcounter)
144         TG_beam.append(TaG / MU_beam)
145         F_beam.append(F / MU_beam)
146         counter += 1
147
148         MCS_arc = 0.
149         if A > 1:
150             for i in range(0, A - 1):
151                 MCS_arc += (Li_AAV[i] + Li_AAV[i + 1]) * (Li_LSV[i]
    + Li_LSV[i + 1]) * 0.25 * Li_MU[i]
152             MCS.append(MCS_arc)
153         MU_beams.append(beam.BeamMU)
154
155     MCS_plan = sum(multiply(MCS, MU_beams)) / sum(MU_beams)
156
157     totaldose = plan.PlanOptimizations[0].
```

```
    PlanningPhaseDoseDependencies[0].RadiationSetSource.FractionDose
    .ForBeamSet.Prescription.PrimaryPrescriptionDoseReference.
    DoseValue
158     fractions = plan.PlanOptimizations[0].
    PlanningPhaseDoseDependencies[0].RadiationSetSource.FractionDose
    .ForBeamSet.FractionationPattern.NumberOfFractions
159     fractiondose = int(int(totaldose) / int(fractions))
160 
161     mu_cGy = beam_mu / fractiondose
162     F = mean(F_beam)
163     TaG = mean(TG_beam)
164     loops_ges = mean(loops)
165 
166     energy = int(beam.BeamQualityId)
167     return [F, TaG, loops_ges, MCS_plan, mu_cGy, totaldose,
    fractions, fractiondose, plan_name, energy, counter]
168 
169 [F, TaG, loops_ges, MCS_plan, mu_cGy, totaldose, fractions,
    fractiondose, plan_name, energy, counter] = getQAParameters()
170 result_params = getQAParameters()
171 result_labels = ["A/U", "TaG", "Loop", "MCS", "MU/cGy", "Total Dose
    ", "Fractions", "Fraction Dose", "Plan Name", "Energy", "Counter
    "]
172 output_string = "\n".join([f"{label}: {value:.3f}" if isinstance(
    value, float) else f"{label}: {value}" for label, value in zip(
    result_labels, result_params)])
173 
174 write_to_file('M:\\Master_Auswertung\\HNO\\HNO_5\\2_GS\\240_IT\\
    MCS_HNO5_2GS_240IT.txt', output_string)
```

Listing 8.3: Python example

List of Figures

Bibliography

[1] RaySearch Laboratories AB. *RayStation 12A: A Guide to Optimization in RayStation*. Version 1.0. Document Number: RSL-D-RS-12A-OPT-EN-1.0-2022-06-23. Stockholm, Sweden, June 2022.

[2] RaySearch Laboratories AB. *VMAT Optimization in RayStation*. Tech. rep. Version 2017-04-20. Simultaneous optimization of two arcs using the dual arc feature. Stockholm, Sweden: RaySearch Laboratories AB, Apr. 2017. URL: https://www.raysearchlabs.com.

[3] ScandiDos AB. *Delta4 Phantom+ Brochure*. Available at: https://delta4family.com. ScandiDos AB. Uppsala Science Park, SE-751 83 Uppsala, Sweden, July 2023.

[4] Andreas Altendorfer. "Utilising elekta LINAC and MLC controller log files for phantom-less patient specific IMRT QA". en. In: *TUWien* (2017). DOI: 10.34726/HSS.2017.31780. URL: https://repositum.tuwien.at/handle/20.500.12708/3798.

[5] Maria Atiq et al. "Interpretation of Gamma Index for Quality Assurance of Simultaneously Integrated Boost (SIB) IMRT Plans for Head and Neck Carcinoma". In: *Polish Journal of Medical Physics and Engineering* 23.4 (Dec. 2017), pp. 93–97. ISSN: 1898-0309. DOI: 10.1515/pjmpe-2017-0016. URL: http://dx.doi.org/10.1515/pjmpe-2017-0016.

[6] Ans Baeyens et al. "Basic Concepts of Radiation Biology". In: *Radiobiology Textbook*. Springer International Publishing, 2023, pp. 25–81. ISBN: 9783031188107. DOI: 10.1007/978-3-031-18810-7_2. URL: http://dx.doi.org/10.1007/978-3-031-18810-7_2.

[7] J. P. Balog et al. “Multileaf collimator interleaf transmission”. In: *Medical Physics* 26.2 (Feb. 1999), pp. 176–186. ISSN: 2473-4209. DOI: 10.1118/1.598501. URL: http://dx.doi.org/10.1118/1.598501.

[8] Woong Cho et al. “Practical implementation of a collapsed cone convolution algorithm for a radiation treatment planning system”. In: *Journal of the Korean Physical Society* 61.12 (Dec. 2012), pp. 2073–2083. ISSN: 1976-8524. DOI: 10.3938/jkps.61.2073. URL: http://dx.doi.org/10.3938/jkps.61.2073.

[9] Wikipedia contributors. *Querprofil (Strahlentherapie)*. Accessed: 2024-08-30. 2024. URL: https://de.wikipedia.org/wiki/Querprofil_(Strahlentherapie).

[10] Sasa Mutic Daniel Low William Harms and James A Purdy. “A technique for the quantitative evaluation of dose distributions”. In: *Medical Physics* (Mar. 1998).

[11] DATAtab. *Pearson Korrelation einfach erklärt*. Accessed: 2024-08-30. 2024. URL: https://datatab.de/tutorial/pearson-korrelation.

[12] Stefanos Diamantopoulos et al. “Treatment plan verification: A review on the comparison of dose distributions”. In: *Physica Medica* 67 (Nov. 2019), pp. 107–115. ISSN: 1120-1797. DOI: 10.1016/j.ejmp.2019.10.029. URL: http://dx.doi.org/10.1016/j.ejmp.2019.10.029.

[13] *Dose Calculation Algorithms*. URL: https://oncologymedicalphysics.com/dose-calculation-algorithms/. accessed: 05.06.2024.

[14] Elekta AB. *Versa HD Brochure*. LPCVHD190103. Stockholm, Sweden, 2019. URL: https://www.elekta.com.

[15] Kara Ferachi. “Multileaf collimator positional reproducibility evaluated with a two-dimensional diode array”. PhD thesis. Louisiana State University Libraries. DOI: 10.31390/gradschool_theses.2857. URL: http://dx.doi.org/10.31390/gradschool_theses.2857.

[16] PTW Freiburg GmbH. *OCTAVIUS 4D: Benefits and Clinical Applications*. Document Number: D913.139.04/00. Freiburg, Germany, Oct. 2020. URL: https://www.ptwdosimetry.com.

[17] Julia Götstedt, Anna Karlsson Hauer, and Anna Bäck. "Development and evaluation of aperture-based complexity metrics using film and EPID measurements of static MLC openings". In: *Medical Physics* 42.7 (June 2015), pp. 3911–3921. ISSN: 2473-4209. DOI: 10.1118/1.4921733. URL: http://dx.doi.org/10.1118/1.4921733.

[18] David Greene and P.C Williams. *Linear Accelerators for Radiation Therapy*. Aug. 2017. DOI: 10.1201/9780429246562. URL: http://dx.doi.org/10.1201/9780429246562.

[19] William R. Hendee and Geoffrey S. Ibbott. *Radiation Therapy Physics*. 3rd. Hoboken, NJ: Wiley-Liss, 2005, pp. 23–35. ISBN: 978-0471661136.

[20] *History of radiation therapy*. URL: https://de.wikipedia.org/wiki/Strahlentherapie#Geschichte_der_Strahlentherapie. accessed: 03.04.2024.

[21] Norfried Thesen Horst Sack. *Bestrahlungsplanung*. ISBN-10: 3137850029. Thieme, 1993. ISBN: 9783137850021.

[22] M. Hussein, C.H. Clark, and A. Nisbet. "Challenges in calculation of the gamma index in radiotherapy – Towards good practice". In: *Physica Medica* 36 (Apr. 2017), pp. 1–11. ISSN: 1120-1797. DOI: 10.1016/j.ejmp.2017.03.001. URL: http://dx.doi.org/10.1016/j.ejmp.2017.03.001.

[23] Mohammad Hussein et al. "A comparison of the gamma index analysis in various commercial IMRT/VMAT QA systems". In: *Radiotherapy and Oncology* 109.3 (Dec. 2013), pp. 370–376. ISSN: 0167-8140. DOI: 10.1016/j.radonc.2013.08.048. URL: http://dx.doi.org/10.1016/j.radonc.2013.08.048.

[24] International Atomic Energy Agency. *Patient Specific Physics QA for IMRT*. Accessed: 2024-09-05. 2023. URL: https://humanhealth.iaea.org/HHW/RadiationOncology/Treatingpatients/Treatment_planning_and_techniques/Training_Course/19_Patient_Specific_Physics_QA_for_IMRT.pdf.

[25] S. Ishikura. "Quality Assurance of Radiotherapy in Cancer Treatment: Toward Improvement of Patient Safety and Quality of Care". In: *Japanese Journal of Clinical Oncology* 38.11 (Sept. 2008), pp. 723–729. ISSN: 1465-3621. DOI: 10.1093/jjco/hyn112. URL: http://dx.doi.org/10.1093/jjco/hyn112.

[26] Subramania Jayaraman and Lawrence H. Lanzl. *Clinical Radiotherapy Physics*. Springer Berlin Heidelberg, 2004, pp. 70–81. ISBN: 9783642185496. DOI: 10.1007/978-3-642-18549-6. URL: http://dx.doi.org/10.1007/978-3-642-18549-6.

[27] Fait M. Kahn. *The Physics of Radiation Therapy*. 1st. Baltimore, MD: Williams & Wilkins, 1984.

[28] Victor Löf. "The Difference Between a Collapsed Cone Based and a Monte Carlo Based Dose Calculation Algorithm". In: 2015. URL: https://api.semanticscholar.org/CorpusID:117167511.

[29] Laura Masi et al. "Impact of plan parameters on the dosimetric accuracy of volumetric modulated arc therapy". In: *Medical Physics* 40.7 (June 2013). ISSN: 2473-4209. DOI: 10.1118/1.4810969. URL: http://dx.doi.org/10.1118/1.4810969.

[30] Andrea L. McNiven, Michael B. Sharpe, and Thomas G. Purdie. "A new metric for assessing IMRT modulation complexity and plan deliverability". In: *Medical Physics* 37.2 (Jan. 2010), pp. 505–515. ISSN: 2473-4209. DOI: 10.1118/1.3276775. URL: http://dx.doi.org/10.1118/1.3276775.

[31] Ivaylo Mihaylov, Bruce Curran, and Edward Sternick. "The effect of gantry spacing resolution on plan quality in a single modulated arc optimization". In: *Journal of applied clinical medical physics / American College of Medical Physics* 12 (Nov. 2011), p. 3603. DOI: 10.1120/jacmp.v12i4.3603.

[32] Uwe Oelkfe and Christian Scholz. "Dose Calculation Algorithms". In: *Medical Radiology*. Springer-Verlag, pp. 187–196. ISBN: 3540003215. DOI: 10.1007/3-540-29999-8_15. URL: http://dx.doi.org/10.1007/3-540-29999-8_15.

[33] QualiFormed. *LINAC Watch - Real-Time LINAC Monitoring System*. Accessed: 2024-08-26. 2024. URL: https://www.qualiformed.com/linacwatch?tid=1.

[34] Raystation. *Raystation 12A Reference Manual Workspace Main version a727*. 12A. 2022, pp. 53–127.

[35] Jalil ur Rehman et al. “Intensity modulated radiation therapy: A review of current practice and future outlooks”. In: *Journal of Radiation Research and Applied Sciences* 11.4 (Oct. 2018), pp. 361–367. ISSN: 1687-8507. DOI: 10.1016/j.jrras.2018.07.006. URL: http://dx.doi.org/10.1016/j.jrras.2018.07.006.

[36] Wolfram Research. *Klein-Nishina Formula for Compton Effect*. Wolfram Demonstrations Project. accessed: 30.07.2024. Accessed 2024. URL: https://demonstrations.wolfram.com/KleinNishinaFormulaForComptonEffect/.

[37] Amarjit S. Saini and Timothy C. Zhu. “Temperature dependence of commercially available diode detectors”. In: *Medical Physics* 29.4 (Mar. 2002), pp. 622–630. ISSN: 2473-4209. DOI: 10.1118/1.1461842. URL: http://dx.doi.org/10.1118/1.1461842.

[38] E. Scherer and H. Sack. *Strahlentherapie, Radiologische Onkologie*. 4th. Springer, 2014, pp. 14–15.

[39] *Strahlentherapie: Radiologische Onkologie*. Springer Berlin Heidelberg, 1996, pp. 110–115. ISBN: 9783642794322. DOI: 10.1007/978-3-642-79432-2. URL: http://dx.doi.org/10.1007/978-3-642-79432-2.

[40] Sun Nuclear Corporation. *ArcCheck*. Accessed: August 8, 2024. 2024. URL: https://www.sunnuclear.com/products/arccheck.

[41] A. Taylor. “Intensity-modulated radiotherapy - what is it?” In: *Cancer Imaging* 4.2 (2004), pp. 68–73. ISSN: 1470-7330. DOI: 10.1102/1470-7330.2004.0003. URL: http://dx.doi.org/10.1102/1470-7330.2004.0003.

[42] Motohiro Uo, Takahiro Wada, and Tomoko Sugiyama. “Applications of X-ray fluorescence analysis (XRF) to dental and medical specimens”. In: *Japanese Dental Science Review* 51.1 (Feb. 2015), pp. 2–9. ISSN: 1882-7616. DOI: 10.1016/j.jdsr.2014.07.001. URL: http://dx.doi.org/10.1016/j.jdsr.2014.07.001.

[43] Elke Van de Casteele. “Model-based approach for beam hardening correction and resolution measurements in microtomography”. In: (Jan. 2004), p. 26.

[44] S Webb. "The physical basis of IMRT and inverse planning". In: *British Journal of Radiology* 76.910 (Mar. 2014), pp. 678–689. ISSN: 0007-1285. DOI: 10.1259/bjr/65676879. eprint: https://academic.oup.com/bjr/article-pdf/76/910/678/54718468/bjr_65676879.pdf. URL: https://doi.org/10.1259/bjr/65676879.

[45] Markus Wendling et al. "A fast algorithm for gamma evaluation in 3D". In: *Medical Physics* 34.5 (Apr. 2007), pp. 1647–1654. ISSN: 2473-4209. DOI: 10.1118/1.2721657. URL: http://dx.doi.org/10.1118/1.2721657.

[46] Medizinphysik Wiki. *Teletherapie - Bestrahlungstechniken*. Accessed: 2024-08-30. 2024. URL: https://medizinphysik.wiki/teletherapie/bestrahlungstechniken/.

[47] *Xray spectrum and the characteristic lines*. URL: https://physicsopenlab.org/2018/02/13/x-ray-emission/. accessed: 29.05.2024.